iScience

CellPress
OPEN ACCESS

Article

Atractylodin modulates ASAH3L to improve galactose metabolism and inflammation to alleviate acute lung injury

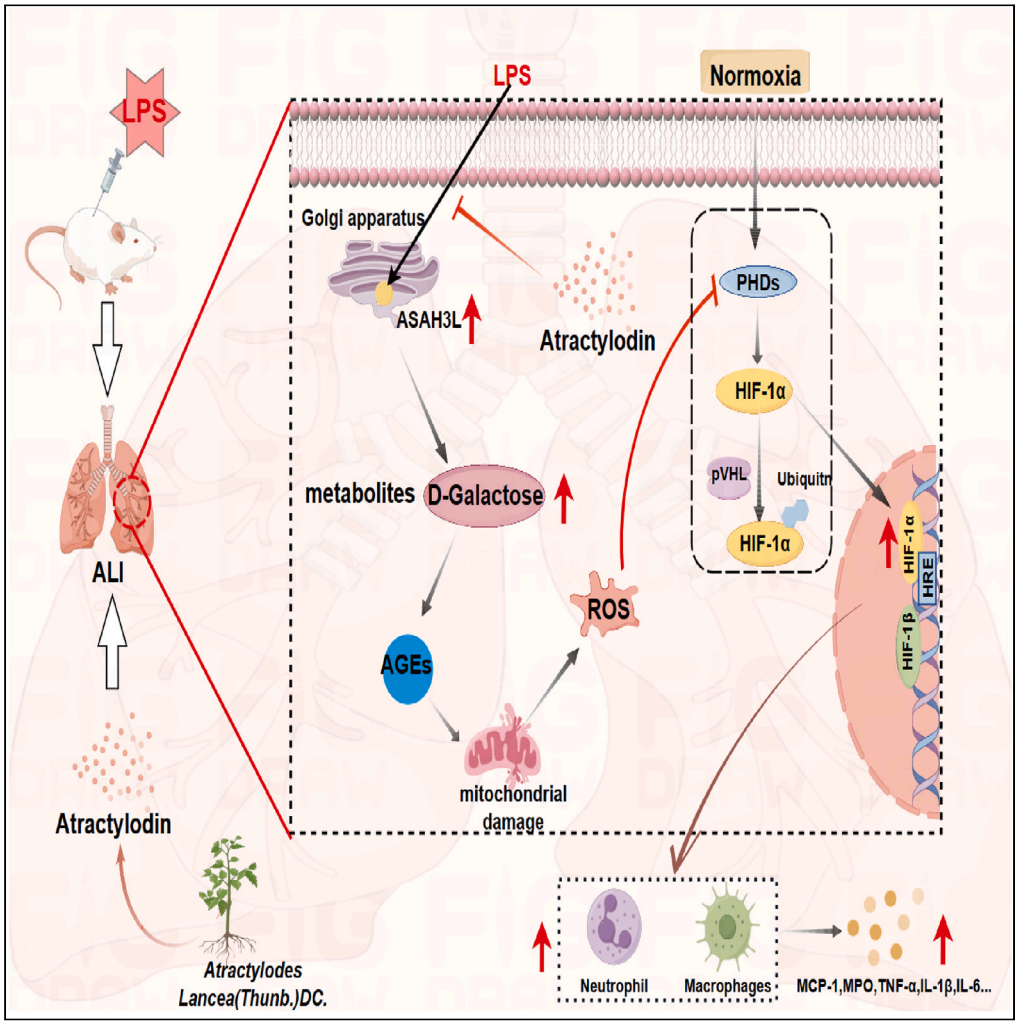

Kun Shi, Yangxin Xiao, Mumujiang Qu, ..., Chang Ke, Linghang Qu, Yanju Liu

linghqu06@hbtcm.edu.cn (L.Q.)
lyj1965954@hbtcm.edu.cn (Y.L.)

Highlights

ATL can regulate galactose metabolism to treat acute lung injury

ASAH3L is a key target for the treatment of acute lung injury with atractylodin

ATL targets ASAH3L to regulate galactose metabolism for acute lung injury

ATL target ASAH3L to inhibit the HIF-1 signaling pathway for acute lung injury

Shi et al., iScience 27, 110751
October 18, 2024
https://doi.org/10.1016/j.isci.2024.110751

iScience

CellPress
OPEN ACCESS

Article

Atractylodin modulates ASAH3L to improve galactose metabolism and inflammation to alleviate acute lung injury

Kun Shi,[1,2,3,4] Yangxin Xiao,[1,2,3,4] Mumujiang Qu,[1] Ying Xie,[1] Yan Wang,[1] Chang Ke,[1] Linghang Qu,[1,2,3,*] and Yanju Liu[1,2,3,5,*]

SUMMARY

Acute lung injury (ALI) is a lung disease characterized by an excessive inflammatory response and damage to lung epithelial cells. Atractylodin (ATL) has good anti-inflammatory activity and protects the integrity of the epithelial cell barrier. However, the efficacy of ATL in the treatment of ALI and its mechanism is unclear. We investigated the efficacy of ATL in treating ALI and explored its targets and mechanisms. The results showed that ATL significantly reduced the wet-dry ratio of lungs of rats with ALI, improved the pathological changes, and lowered the expression of the inflammatory factors. Combined metabolomic and transcriptomic analyses showed that ATL can reduce inflammation by inhibiting and activating the HIF-1 signaling pathway and modulating ASAH3L to improve galactose metabolism, thereby alleviating ALI. In conclusion, ATL may be a potential drug for the treatment of acute lung injury.

INTRODUCTION

Acute lung injury (ALI) is an acute hypoxic respiratory insufficiency caused by damage to alveolar epithelial cells and capillary endothelial cells because of various direct and indirect injury-causing factors, which result in diffuse interstitial and alveolar edema.[1,2] Pathophysiological features of reduced lung volume, reduced lung compliance, and ventilation/blood flow ratio imbalance are clinically manifested by progressive hypoxemia and respiratory distress, with non-homogeneous exudative lesions on lung imaging.[3,4] Without prompt and effective treatment, ALI can further develop into acute respiratory distress syndrome, which is seriously life threatening. Currently, drug treatments for ALI are mainly based on glucocorticoids, including dexamethasone, prednisolone, and ustekin.[5] However, all these drugs cause different degrees of adverse effects, such as coagulation dysfunction, gastric ulcers, and osteoporosis.[6] Therefore, seeking new therapeutic drugs with fewer side effects is of particular importance.

When ALI occurs, patients experience dyspnea leading to hypoxia, which is one of the main factors regulating HIF-1.[7] HIF-1 was originally extracted from the nucleus during a study evaluating hypoxia-induced erythropoietin gene expression. It is a transcriptionally active nuclear protein comprising two subunits (HIF-1α and HIF-1β), and is present in almost all cells, with the HIF-1α subunit playing a major role.[8] Some studies have reported that HIF-1α can directly promote the expression of multiple inflammatory factors under hypoxic conditions, causing tissue and organ damage, and the expression of multiple inflammatory factors further promotes the expression of HIF-1α, thus forming a positive feedback pro-inflammatory effect, amplifying the inflammatory response and further exacerbating lung injury.[9,10]

Diseases always cause abnormal changes in the metabolism, function, and morphology of living organisms. Moreover, metabolism, as the basis of function and morphology, is an important indicator of the occurrence of many diseases.[11,12] The application of metabolomics allows for the speculation of altered endogenous metabolites and aberrant metabolic pathways to elucidate the mechanism of drug action. Numerous studies have shown that Chinese herbs can alleviate ALI by modulating multiple metabolic pathways, such as galactose metabolism, amino acid metabolism, and lipid metabolism, to reduce inflammation.[13–15]

In recent years, researchers in China and overseas have conducted a large number of detailed studies on the pathological damage induced by ALI and molecular mechanisms of ALI development and found that various active ingredients of traditional Chinese medicine can play a pharmacological role in preventing and controlling ALI through different pathways of action.[16,17] Atractylodin (ATL) is one of the main active constituents of Atractylodes lancea (Thunb.) DC, which has good anti-inflammatory effects and protects the integrity of the epithelial barrier.[18–20] Some studies have shown that ATL can inhibit TGF-β-induced pneumonia and pulmonary fibrosis.[21] However,

[1]College of Pharmacy, Hubei University of Chinese Medicine, Wuhan 430065, China
[2]Center for Hubei TCM Processing Technology Engineering, Wuhan 430065, China
[3]Hubei Shizhen Laboratory, Wuhan 430065, China
[4]These authors contributed equally
[5]Lead contact
*Correspondence: linghqu06@hbtcm.edu.cn (L.Q.), lyj1965954@hbtcm.edu.cn (Y.L.)
https://doi.org/10.1016/j.isci.2024.110751

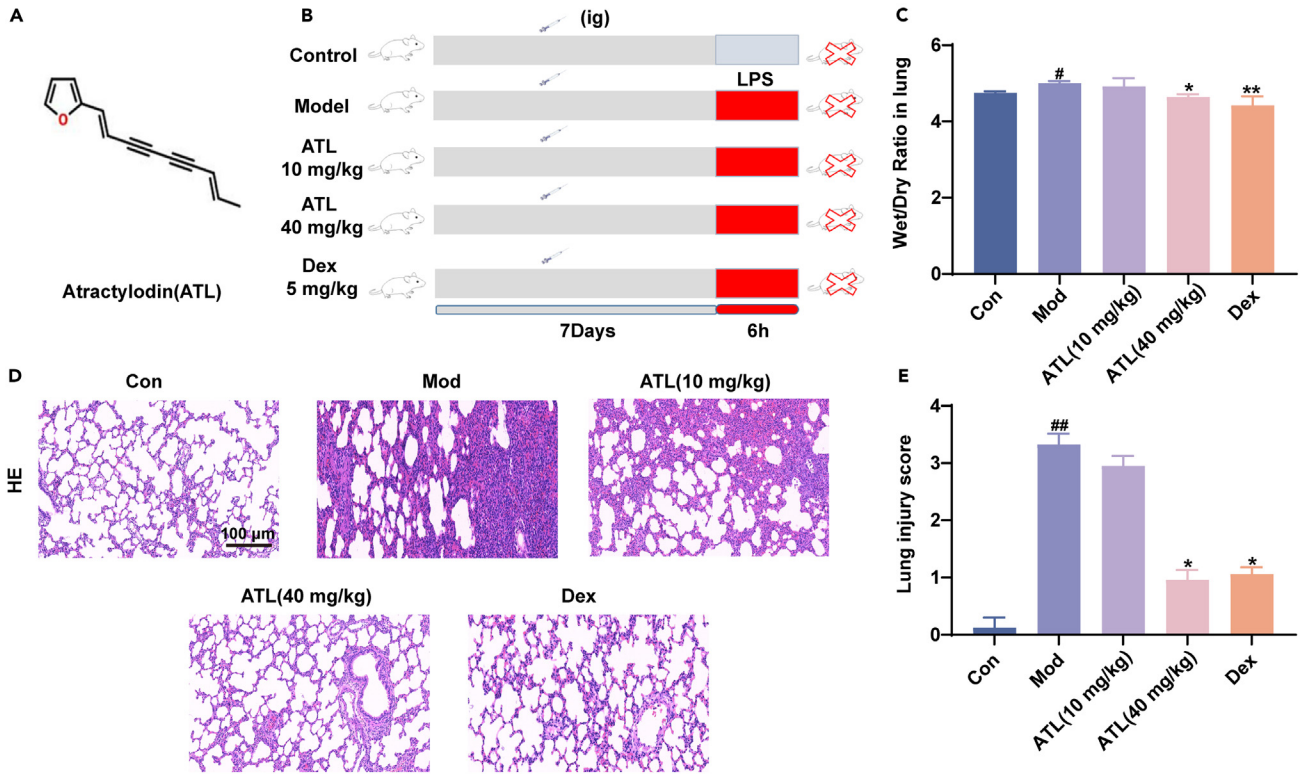

Figure 1. ATL can improve the W/D ratio and pathological changes in the lungs of rats with ALI

(A) Structure of ATL.

(B) Experimental process flow chart.

(C) Lung W/D ratio.

(D) Hematoxylin-eosin staining of the lung tissue.

(E) The statistical chart of lung injury scores. The data are expressed as mean ± SEM, $n = 6$. $^{\#}p < 0.05$ and $^{\#\#}p < 0.01$ vs. Control; $^{*}p < 0.05$ and $^{**}p < 0.01$ vs. Model.

the mechanism of ATL treatment for ALI has not been fully studied. Therefore, our study delves into the efficacy and mechanism of ATL in treating ALI, aiming to provide a basis for the development of new drugs for treating ALI.

RESULTS

Atractylodin improves wet/dry ratio and pathological changes of lungs in acute lung injury rats

The ALI model (Figure 1B) was induced by a tracheal drip of LPS (5 mg/kg) after rats were given different doses of ATL gavage for 7 days. As shown in Figure 1C, the W/D ratio of the lungs of the rats in the model group was significantly higher than that of the lungs of the rats in the control group. After treatment with ATL, there was a significant decrease in the W/D ratio of the lungs in both the ATL (40 mg/kg) and Dex groups compared with the model group. On analyzing the H&E sections, we found that rats in the model group showed significant alveolar atrophy, alveolar wall thickening, and inflammatory cell infiltration compared with the rats in the control group, and these pathological changes were significantly ameliorated in both the ATL (40 mg/kg) and Dex groups (Figures 1D and 1E).

Atractylodin reduces the expression of inflammatory factors in the lungs

We examined inflammatory factors in BALF as well as in the lung tissue. The results of RT-PCR showed that the mRNA levels of inflammatory factors (TNF-α, IL-1β, IL-6, COX-2, and INOS) were significantly higher in the lung tissues of the model group than in those of the control group. After medication administration, there was a decrease to varying degrees, with more significant effects in the ATL group (40 mg/kg) and the Dex group (Figures 2A–2E). In addition, we found similar results in the BALF (Figures 2F–2J). By immunohistochemical analysis, we found that the expression of MPO and MCP-1 was significantly elevated in the model group compared with the control group, and the most significant decreases were observed in the ATL (40 mg/kg) and Dex groups after treatment administration (Figures 2K–2N).

Atractylodin reduces neutrophil and macrophage aggregation and activation in the lungs

It has been shown that the excessive aggregation and activation of neutrophils and macrophages in the lungs are closely associated with ALI development.[22] Accordingly, we examined neutrophils and macrophages in the lung tissue by immunofluorescence staining. The results

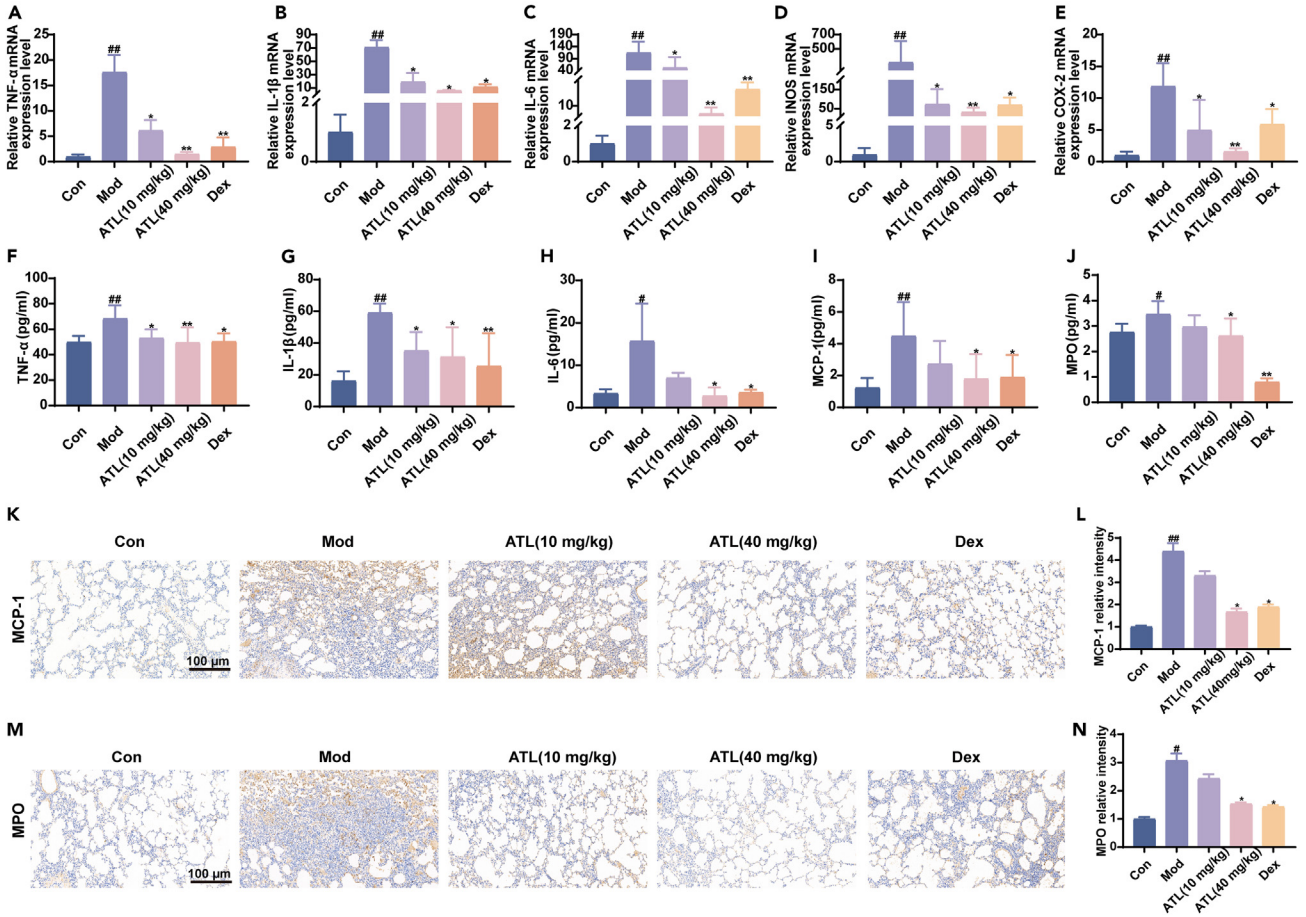

Figure 2. ATL decreased inflammatory factors in the lungs of ALI rats

The relative mRNA expression of (A) TNF-α, (B) IL-1β, (C) IL-6, (D) INOS, and (E) COX-2 in lung tissues. The levels of (F) TNF-α, (G) IL-1β, (H) IL-6, and (I) MCP-1 in BALF as determined by ELISA.

(J) The levels of MPO in lung tissues as determined by ELISA.

(K) Immunohistochemical staining of MCP-1.

(L) Immunohistochemistry statistics of MCP-1.

(M) Immunohistochemical staining of MPO.

(N) Immunohistochemistry statistics of MPO. The data are expressed as mean ± SEM, $n = 6$. $^{\#}p < 0.05$ and $^{\#\#}p < 0.01$ vs. Control; $^{*}p < 0.05$ and $^{**}p < 0.01$ vs. Model.

showed that the levels of neutrophils and macrophages were significantly increased in the model group compared with the control group. After being treated with ATL, these levels were reduced to different degrees in the lung tissues, with the most significant decreases observed in the ATL (40 mg/kg) and Dex groups (Figures 3A–3D).

Atractylodin inhibits the expression of inflammatory factors in THP-1 cells

In order to further validate the efficacy of ATL, we induced inflammation in THP-1 cells *in vitro* using LPS to simulate a model of ALI.[23] First, we found no significant cytotoxicity of ATL below 80 μM via the CCK-8 assay (Figure 4A). Accordingly, we determined the administration concentrations of ATL as 10 μM, 20 μM, and 40 μM. In the *in vitro* cellular assay, the expression levels of inflammatory factors TNF-α, IL-1β, IL-6, and MCP-1 were significantly higher in the model group than in the control group. There was a significant decrease in the levels of these factors (Figures 4B–4H) after the administration of different concentrations of ATL, which is consistent with the results of our *in vivo* experiments. This further demonstrates that ATL has good anti-inflammatory activity.

Transcriptomic analysis of lung tissue

To clarify the mechanism of ATL, we performed transcriptomic analysis of lung tissues from rats in the control, model, and ATL (40 mg/kg) groups. Principal component analysis (PCA) showed that the gene expression levels in the lung tissues of rats in the control and

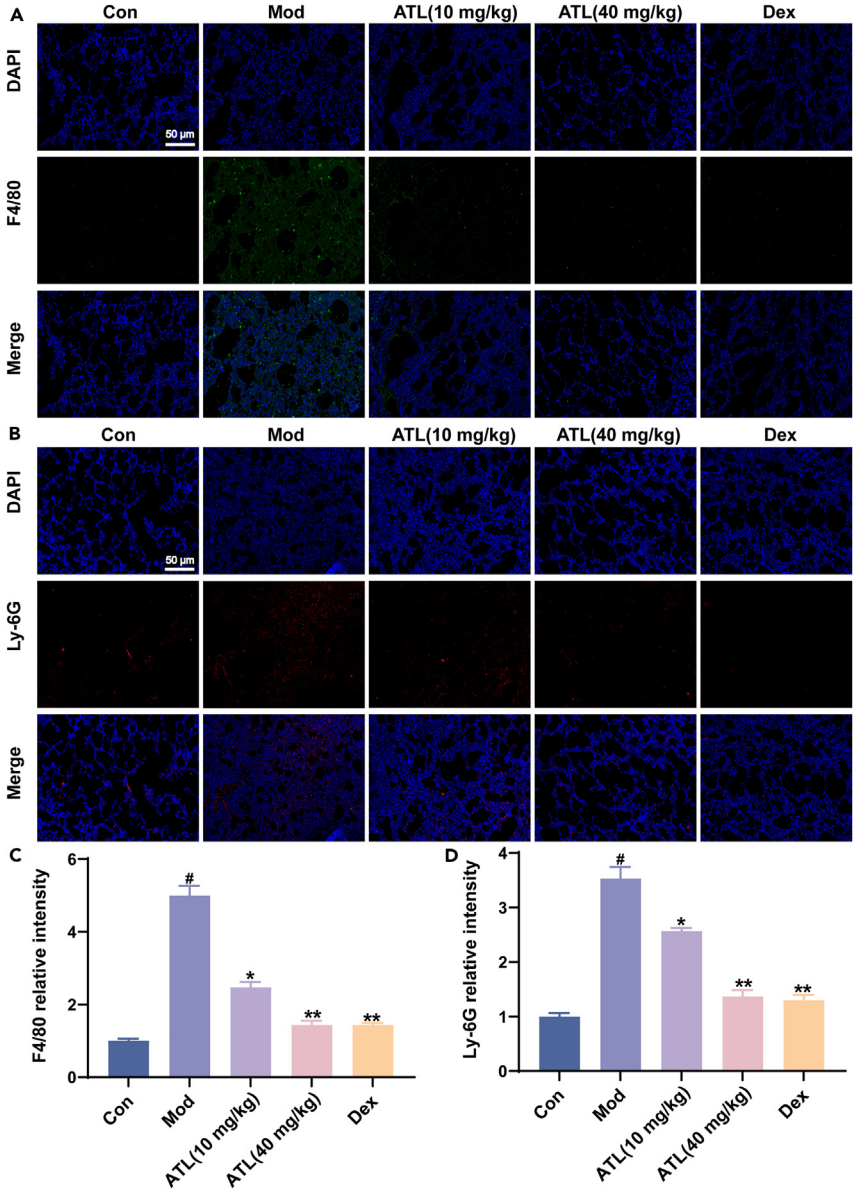

Figure 3. ATL reduces macrophages and neutrophil aggregation and activation in the lungs

(A) Immunefluorescence staining of macrophages in lung tissue for F4/80.

(B) Immunefluorescence staining of neutrophils in lung tissue for Ly-6G.

(C) Immunofluorescence statistics for F4/80.

(D) Immunofluorescence statistics for Ly-6G. The data are expressed as mean ± SEM, $n = 6$. $^{\#}p < 0.05$ vs. Control; $^{*}p < 0.05$ and $^{**}p < 0.01$ vs. Model.

model groups were significantly different, whereas the gene expression levels in the lung tissues of rats in the ATL group (40 mg/kg) were similar to those observed in the control group (Figure 5A). Compared with the control group, the model group showed an upregulation of 666 genes and a downregulation of 814 genes in the lung tissues (Figure 5C). In addition, compared with the model group, 112 genes were up-regulated and 181 genes were down-regulated in the ATL (40 mg/kg) group (Figure 5D). By Venn diagram analysis, 79 genes could be regulated by ATL (Figure 5B). Cluster Heatmap showed that the ATL (40 mg/kg) group and the control group could be clustered together, while the model group was clustered separately (Figure 5E). KEGG analysis revealed that ATL regulated lung tissue differential genes were mainly concentrated in HIF-1 signaling pathway and some glucose metabolism pathways (Figure 5F). GO analysis showed that the genes regulated by ATL are closely related to changes in metabolic processes (Figure 5G).

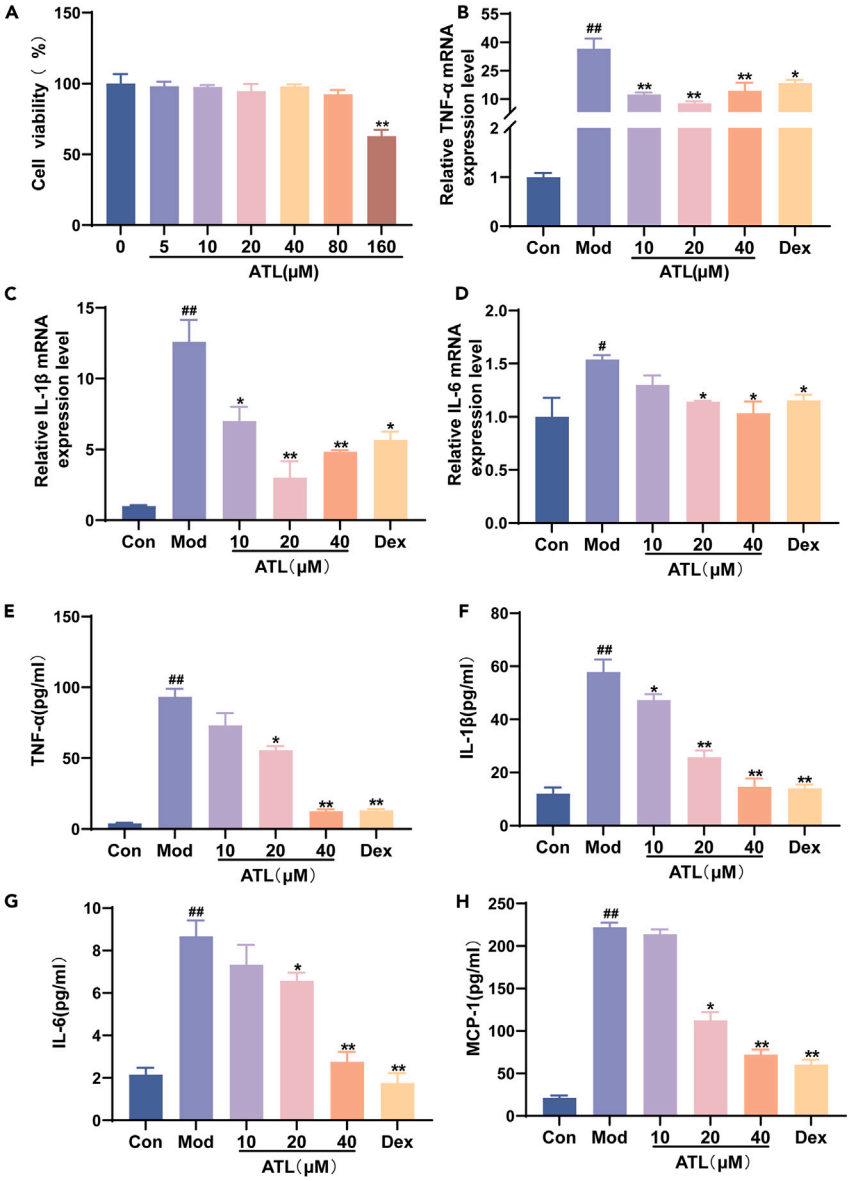

Figure 4. ATL decreases the inflammatory factors in THP-1 cells

(A) Cell viability assay. The relative mRNA expressions of (B) TNF-α, (C) IL-1β, and (D) IL-6 in cells. The levels of (E) TNF-α, (F) IL-1β, (G) IL-6, and (H) MCP-1 in cell supernatants were determined by ELISA. The data are expressed as mean ± SEM, $n = 6$. $^{\#}p < 0.05$ and $^{\#\#}p < 0.01$ vs. Control; $^{*}p < 0.05$ and $^{**}p < 0.01$ vs. Model.

Metabolomic analysis of lung tissues of rats with acute lung injury treated with atractylodin

Because transcriptomics analysis revealed that the mechanism of ATL therapy for ALI was associated with some glucose metabolism pathways, we performed metabolomics analysis of lung tissues from rats in the control, model, and ATL (40 mg/kg) groups (Figure 6A). PCA analyses revealed a significant difference among the control, model, and ATL (40 mg/kg) groups, suggesting a difference between the metabolites of these three groups (Figure 6B). Clustered heatmap analysis similarly showed differences in metabolites between groups (Figure 6C). To clarify the regulatory role of ATL on metabolism, we searched for differential metabolites in ALI by orthogonal projection to latent structures squares discriminant analysis (OPLS-DA) (VIP >1) (Figures 6D and 6E) and T-test ($p < 0.05$) (Figures 6F and 6G). In addition, 100 external experiments demonstrate that our established OPLS-DA model shows good prediction performance (Figures 6H and 6I).

Comparing the control and model groups with $p < 0.05$ and VIP >1 as screening conditions, we gained 47 different metabolites. Likewise, by comparing the model and ATL (40 mg/kg) groups, we gained 53 different metabolites. Further, by intersection analysis of Venn diagrams, we obtained 20 shared differential metabolites (Figure 7A). Subsequently, PCA analysis of these 20 differential metabolites indicated that most of the samples in the control and ATL (40 mg/kg) groups were closer together compared with the samples in the model group. This

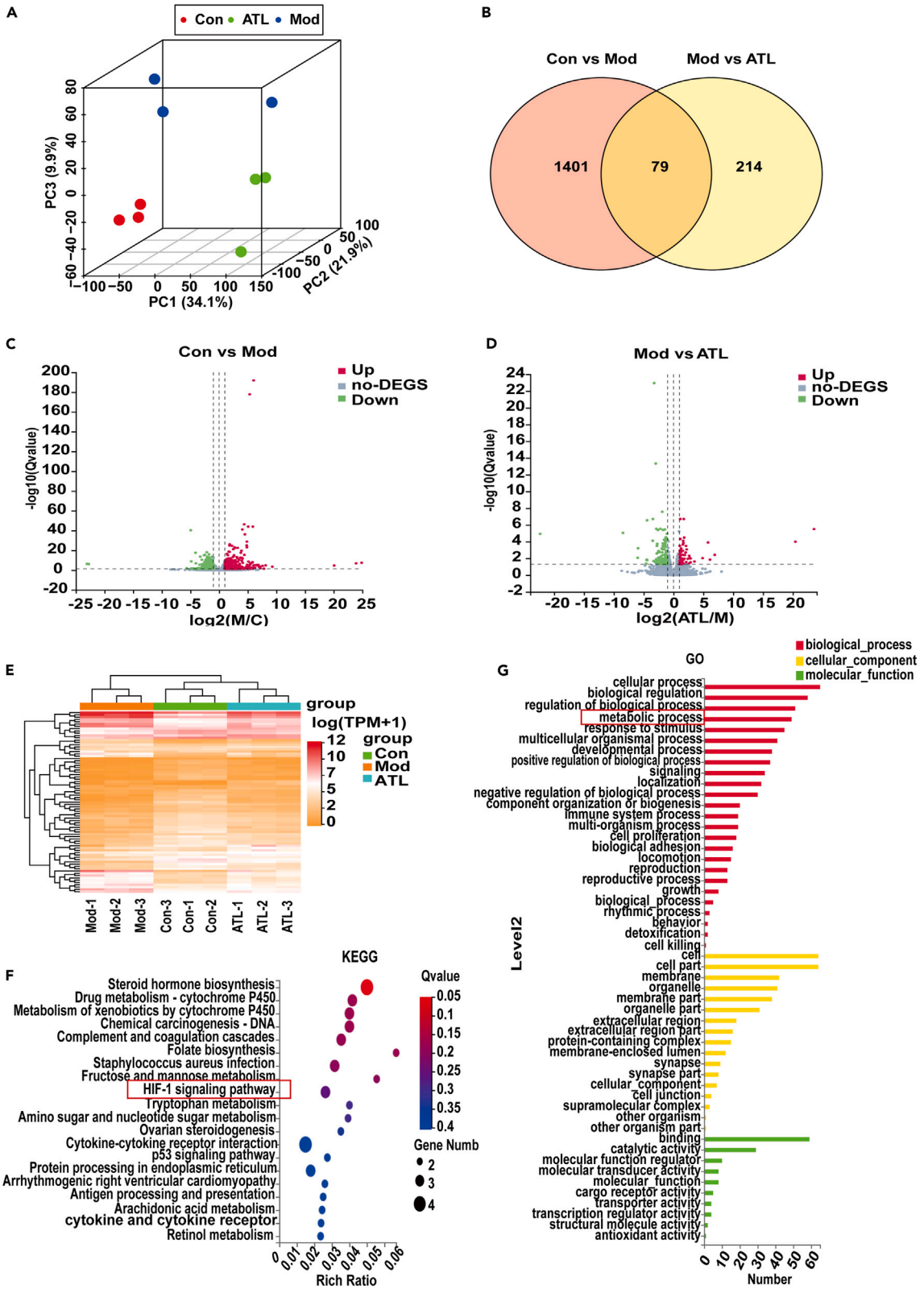
A
Con
ATL
Mod
PC3 (9.9%)
PC1 (34.1%)
PC2 (21.9%)
B
Con vs Mod
Mod vs ATL
1401
79
214
C
Con vs Mod
Up
no-DEGS
Down
-log10(Qvalue)
log2(M/C)
D
Mod vs ATL
Up
no-DEGS
Down
-log10(Qvalue)
log2(ATL/M)
E
group
log(TPM+1)
group
Con
Mod
ATL
Mod-1
Mod-2
Mod-3
Con-3
Con-1
Con-2
ATL-1
ATL-2
ATL-3
F
KEGG
Qvalue
Gene Numb
Steroid hormone biosynthesis
Drug metabolism - cytochrome P450
Metabolism of xenobiotics by cytochrome P450
Chemical carcinogenesis - DNA
Complement and coagulation cascades
Folate biosynthesis
Staphylococcus aureus infection
Fructose and mannose metabolism
HIF-1 signaling pathway
Tryptophan metabolism
Amino sugar and nucleotide sugar metabolism
Ovarian steroidogenesis
Cytokine-cytokine receptor interaction
p53 signaling pathway
Protein processing in endoplasmic reticulum
Arrhythmogenic right ventricular cardiomyopathy
Antigen processing and presentation
Arachidonic acid metabolism
cytokine and cytokine receptor
Retinol metabolism
Rich Ratio
G
GO
biological_process
cellular_component
molecular_function
Level2
cellular process
biological regulation
regulation of biological process
metabolic process
response to stimulus
multicellular organismal process
developmental process
positive regulation of biological process
signaling
localization
negative regulation of biological process
component organization or biogenesis
immune system process
multi-organism process
cell proliferation
biological adhesion
locomotion
reproduction
reproductive process
growth
biological_process
rhythmic process
behavior
detoxification
cell killing
cell
cell part
membrane
organelle
membrane part
organelle part
extracellular region
extracellular region part
protein-containing complex
membrane-enclosed lumen
synapse
synapse part
cellular_component
cell junction
supramolecular complex
other organism
other organism part
binding
catalytic activity
molecular function regulator
molecular transducer activity
molecular_function
cargo receptor activity
transporter activity
transcription regulator activity
structural molecule activity
antioxidant activity
Number

Figure 5. Transcriptomic analysis of lung tissues from rats with ALI treated with ATL

(A) PCA analysis of different groups of genes.
(B) Venn diagram analysis of differential genes in different groups.
(C) Differential gene volcano maps in control and model group rats.
(D) Differential gene volcano maps in model and ATL group rats.
(E) Heatmap analysis of the clustering of differential genes into different groups.
(F) KEGG analysis of 79 shared differential genes.
(G) GO analysis of 79 shared differential genes (n = 3).

finding suggested that these 20 differential metabolites were more similarly expressed in the control and ATL (40 mg/kg) groups (Figure 7B). On further statistically analyzing these 20 differential metabolites, six were found to be significantly different (Figures 7C–7H). Clustering heatmap analysis of these six significantly different metabolites revealed that the control group and the ATL (40 mg/kg) group were essentially clustered into one category (Figure 7I). We performed KEGG enrichment analyses of these six significantly different metabolites and found that the main pathways affected by these six metabolites were lactose degradation, galactose metabolism, and sphingolipid metabolism (Figure 7J).

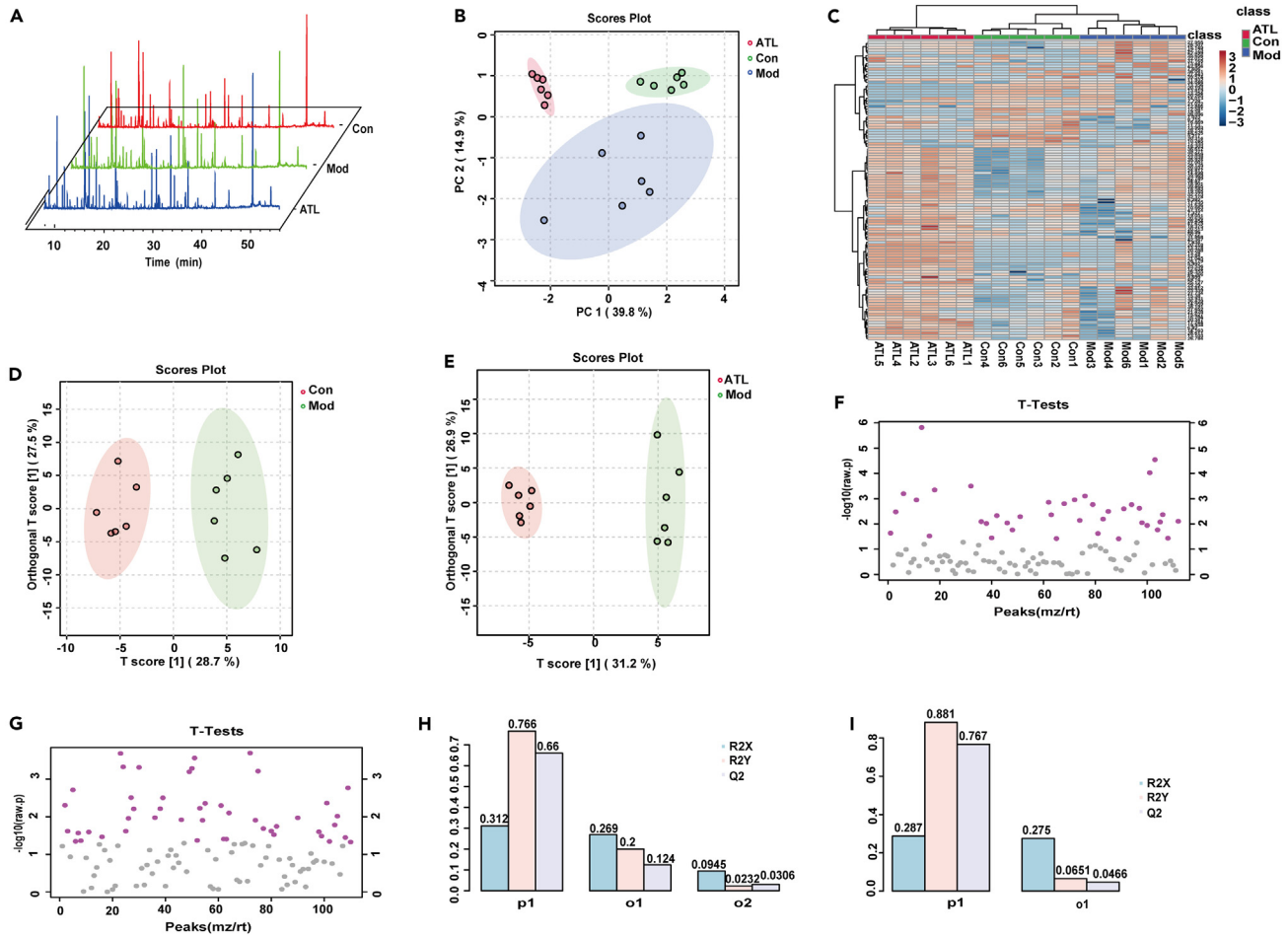

Figure 6. Multiple analyses of metabolite

(A) Metabolic profiles of different groups.
(B) PCA analysis of metabolites from different groups.
(C) Heatmap analysis of clustering of different groups of metabolites.
(D) Metabolites of control vs. model groups by OPLS-DA analysis.
(E) Metabolites of model and ATL groups by OPLS-DA analysis.
(F) Metabolites of control and model groups analyzed by t-test.
(G) Metabolites of model and ATL groups analyzed by t-test.
(H) Validation parameters of the OPLS-DA model for the control vs. model groups.
(I) Validation parameters of the OPLS-DA model for the model and ATL groups. (n = 6).

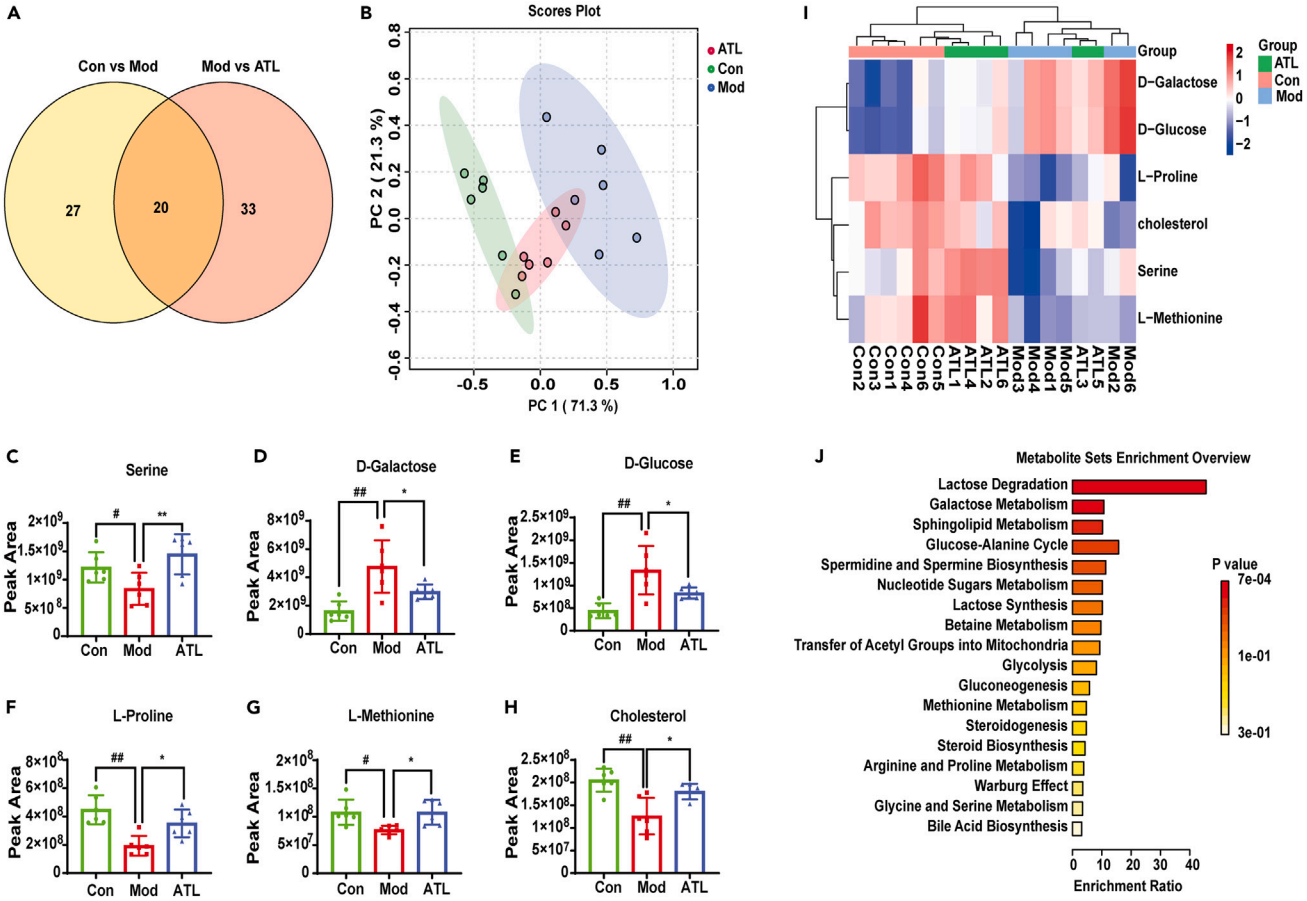

Figure 7. Enrichment analysis of differential metabolites

(A) Venn diagram analysis in different groups.

(B) PCA analysis of 20 shared differential metabolites.

(C–J) Significantly different metabolite expression levels: (C) serine, (D) D-galactose, (E) D-glucose, (F) L-proline, (G) L-methionine, and (H) cholesterol.

(I) Clustered heatmap analysis of six metabolites with significant differences.

(J) Enrichment analysis of six metabolites with significant differences. The data are expressed as mean ± SEM, $n = 6$. $^{\#}p < 0.05$ and $^{\#\#}p < 0.01$ vs. Control; $^{*}p < 0.05$ and $^{**}p < 0.01$ vs. Model.

Association analysis and validation of metabolomics and transcriptomics findings for the treatment of acute lung injury with atractylodin

To clarify the potential molecular mechanisms through which ATL regulates galactose metabolism, we constructed a compound-reaction-enzyme-gene network by importing six significantly different metabolites and 79 differentially expressed genes into the MetScape application of Cytoscape. This analysis then identified an important target gene ASAH3L (Figure 8A). In addition, we examined the HIF-1 signaling pathway by immunofluorescence and Western blotting. Compared with the control group, the expression of HIF-1α was elevated in the model group, and the expression of HIF-1α was significantly reduced in the lung tissues of ALI rats after ATL treatment. (Figures 8B–8E). To validate the predicted results, we detected the protein expression levels of ASAH3L in the lung tissues. ASAH3L expression was significantly increased in the model group compared with the control group, and ASAH3L protein expression levels were significantly reduced in rat lung tissues after ATL treatment (Figures 8F and 8G).

Overexpression experiments confirm that atractylodin ameliorates acute lung injury in rats via ASAH3L

To further clarify whether ATL ameliorates ALI in rats via ASAH3L, we constructed an ASAH3L plasmid and verified whether ATL has a protective effect in rats with overexpression ASAH3L using an ALI model (Figure 9A). The results showed that the ability of ATL to reduce the W/D ratio as well as inflammation in the rats with ALI was reversed after ASAH3L overexpression (Figures 9B–9G). In addition, we semi-quantitatively evaluated the D-galactose content in lung tissues by GC-MS and found that the galactose-reducing effect of ATL was diminished after overexpression of ASAH3L (Figure 9H). To further clarify the effect of ATL on the products of abnormal galactose metabolism, we examined AGEs and found that in the LPS group, the content of AGEs was significantly increased, whereas ATL treatment significantly reduced the

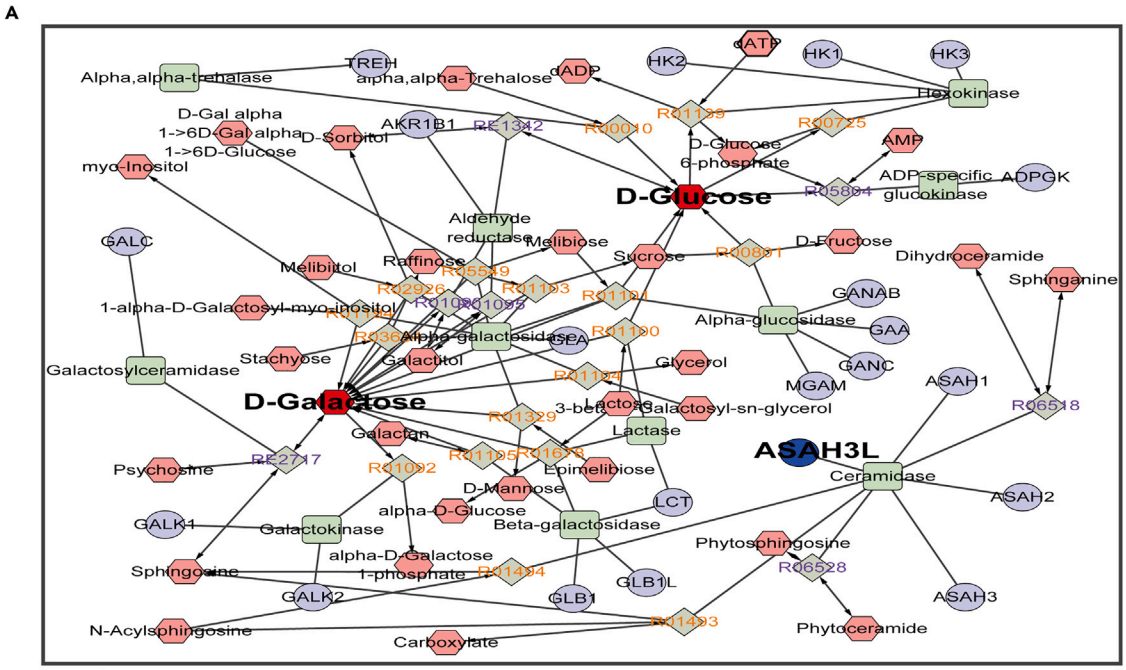
A
Alpha,alpha-trehalase
TREH
alpha,alpha-Trehalose
dADP
dATP
HK2
HK1
HK3
Hexokinase
D-Gal alpha
1->6D-Gal alpha
1->6D-Glucose
myo-Inositol
AKR1B1
D-Sorbitol
RE1342
R00010
R01786
R00725
AMP
D-Glucose
6-phosphate
ADP-specific
glucokinase
ADPGK
R05804
D-Glucose
Aldehyde
reductase
GALC
Melibiose
Sucrose
R00801
D-Fructose
Dihydroceramide
Sphinganine
Melibiitol
Raffinose
R05539
R02926
R01103
R01101
1-alpha-D-Galactosyl-myo-inositol
R01095
R01100
R01102
R01364
Alpha-galactosidase
SEA
Alpha-glucosidase
GANAB
GAA
GANC
MGAM
Stachyose
Galactitol
Glycerol
Galactosylceramidase
R01104
D-Galactose
3-beta
Lactose
Galactosyl-sn-glycerol
R06518
R01329
Galactan
Lactase
ASAH3L
Ceramidase
ASAH1
ASAH2
Psychosine
RE2747
R01092
R01095
R01678
Epimelibiose
D-Mannose
LCT
alpha-D-Glucose
Beta-galactosidase
GALK1
Galactokinase
alpha-D-Galactose
1-phosphate
R01494
Phytosphingosine
R06528
Sphingosine
GLB1L
GALK2
GLB1
ASAH3
R01493
N-Acylsphingosine
Carboxylate
Phytoceramide

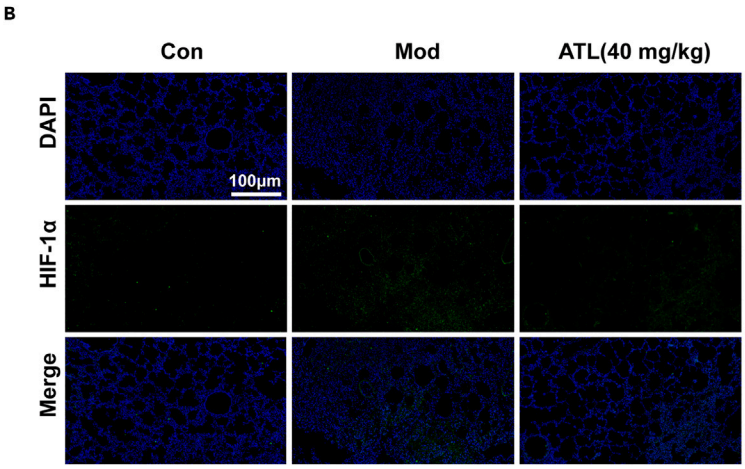
B
Con
Mod
ATL(40 mg/kg)
DAPI
HIF-1α
Merge
100μm

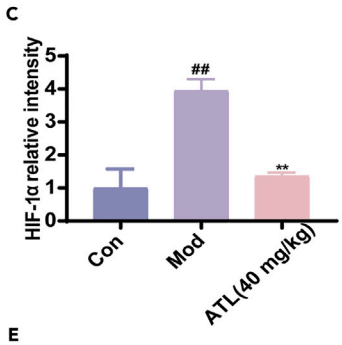
C
HIF-1α relative intensity
##
**
Con
Mod
ATL(40 mg/kg)

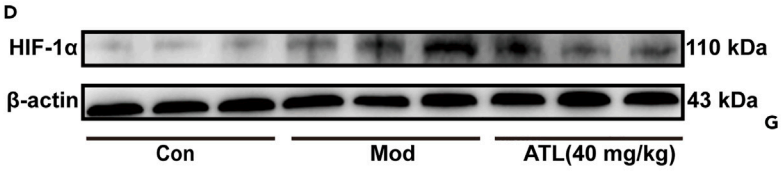
D
HIF-1α
110 kDa
β-actin
43 kDa
Con
Mod
ATL(40 mg/kg)

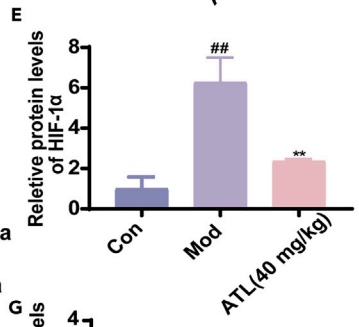
E
Reletive protein levels
of HIF-1α
##
**
Con
Mod
ATL(40 mg/kg)

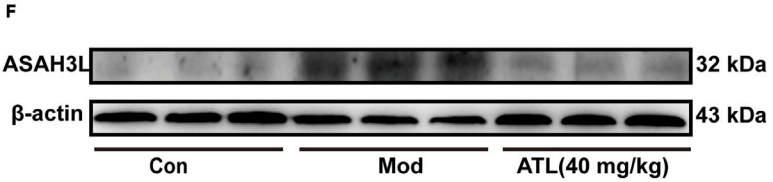
F
ASAH3L
32 kDa
β-actin
43 kDa
Con
Mod
ATL(40 mg/kg)

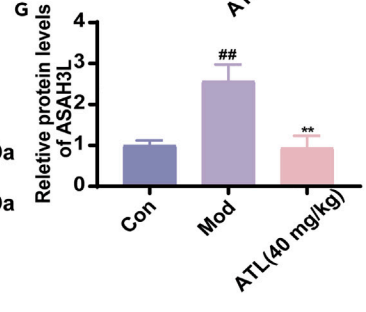
G
Reletive protein levels
of ASAH3L
##
**
Con
Mod
ATL(40 mg/kg)

Figure 8. Association analysis of metabolites associated with galactose metabolism with the help of differential genes

(A) Compound-reaction-enzyme-gene network constructed with the Metscape application of Cytoscape software.

(B) Immunofluorescence staining of HIF-1α.

(C) Immunofluorescence statistics of HIF-1α.

(D) Western blotting of HIF-1α expression in the lung tissue.

(E) Quantitative analysis of HIF-1α levels.

(F) Western blotting of ASAH3L expression in the lung tissue.

(G) Quantitative analysis of ASAH3L levels. The data are expressed as mean ± SEM, $n = 3$. $^{\#\#}p < 0.01$ vs. Control; $^{**}p < 0.01$ vs. Model.

content of AGEs. However, the protective effect of ATL was reversed when ASAH3L was overexpressed (Figure 9I). H&E pathological sections showed the same results (Figure 9J).

To validate the effect of ASAH3L overexpression on HIF-1α and ROS, we examined the expression levels of HIF-1α and ROS using different methods. We found that the inhibition of HIF-1α and ROS expression by ATL was largely counteracted after ASAH3L overexpression (Figures 10A–10D).

DISCUSSION

ALI is defined as an acute, progressive exacerbation of respiratory failure caused by various intrapulmonary and extrapulmonary causative factors other than those of a cardiac origin, and is an inflammatory syndrome of the lungs characterized by increased alveolar capillary permeability.[24] The pathological mechanisms of ALI are more varied and ALI is mostly caused by bacterial endotoxins. LPS is derived from gram-negative bacteria, and its model of induced ALI resembles many aspects of the human ALI disease and is a widely used experimental model. When ALI occurs, it prompts the recruitment and activation of inflammatory cells in the lung tissue, releasing a large number of inflammatory factors, such as chemokines. These inflammatory factors then trigger an inflammatory cascade reaction, forming a "cytokine storm" and ultimately leading to lung tissue damage.[25] In addition, pulmonary edema, as the most important pathological feature in ALI development, has been shown to occur with direct damage to endothelial and epithelial cells of the lungs, the disruption of the alveolar capillary barrier integrity, increased permeability, altered inter-epithelial osmotic gradient, decreased Na^+ active transport activity, and loss of driving force for water reabsorption.[26] Excessive inflammation is one of the main features of ALI, and the damage caused by ALI can be effectively reduced by suppressing the inflammatory response. In this study, we demonstrated that ATL not only reduced the levels of inflammatory factors such as TNF-α, IL-1β, and IL-6 in rats with ALI but also inhibited the expression of inflammatory factors *in vitro*, further proving the anti-inflammatory effects of ATL. In addition, ATL can effectively reduce alveolar atrophy, alveolar wall thickening, and inflammatory cell infiltration in the lungs, reduce the W/D ratio, and alleviate pulmonary edema in rats with ALI. All these results suggest that ATL has a favorable therapeutic effect on ALI.

It has been shown that macrophages and neutrophils play an important role in the development and progression of ALI.[27] Macrophages are the most important regulator of the local inflammatory microenvironment and inflammatory response in the lungs. When the lungs are stimulated by various exogenous pathogenic factors, the immune cells in the lungs are activated and they release a large number of inflammatory mediators, triggering a cascade of amplified inflammatory responses, and macrophage activation is considered to be the initiating factor for ALI.[28] When the body undergoes an inflammatory response, neutrophils are the earliest cells to be recruited to the site of injury, where they can exacerbate tissue damage by releasing proteases. In the case of ALI, these cells also migrate to the lungs to release bactericidal proteins, cytokines, and ROS to perform a wide range of pro-inflammatory functions, critical for the development of ALI.[29,30] Recent studies have shown that MCP-1 is an important pro-inflammatory cytokine, and during the development of ALI, activated macrophages are able to secrete MCP-1 themselves. This tends to increase the number of mononuclear macrophages in the body recruited to the site of inflammation, resulting in increased macrophage accumulation at the site of the lesion, exacerbating the inflammatory response and lesion damage in ALI.[31] Further, MPO, a member of the heme peroxidase family, is a functional and activation marker for neutrophils. In the present study, we found significant aggregation of macrophages and neutrophils in the lungs in the model group, Furthermore, increased expression of MPO and MCP-1 in the lungs also indicated an overactivation of macrophages and neutrophils. In contrast, the administration of ATL significantly reduced the over-aggregation and activation of macrophages and neutrophils in the lungs and alleviated the ALI.

HIF-1 is widely found in a variety of cells, maintains oxygen homeostasis within the body, and is involved in the regulation of inflammatory responses within the body.[32] Under normoxia, the oxygen-dependent degradation structural domain (ODDD) of the HIF-1 is hydroxylated by prolyl hydroxylases (PHDs) and rapidly degraded via the ubiquitin proteasome route. Under hypoxic conditions, mitochondrial electron transport is inhibited, generating a large amount of ROS, which inhibits PHD activity, leading to an increase in the expression of HIF-1α because of the inhibition of HIF-1α degradation.[33] In turn, HIF-1α forms a dimer with HIF-1β and activates target gene transcription.[34] During ALI, the lungs are in a state of hypoxia, and the alveolar epithelial cells activate the expression of HIF-1α and the inflammatory chain because of stress factors and hypoxic damage.[8] This ultimately leads to increased capillary permeability with microthrombosis, alveolar membrane damage, increased alveolar exudation, and the formation of pulmonary edema.[35] Our transcriptome enrichment analysis revealed that the mechanism of ATL in preventing ALI was mainly focused on the HIF-1 signaling pathway and multiple metabolic pathways, while further experimental validation showed that ATL could inhibit the expression of HIF-1α. We, therefore, suggest that ATL alleviates lung injury by inhibiting the HIF-1 signaling pathway and thereby reducing inflammation.

Currently, metabolomics has been widely used to study disease-related targets and is an important tool for identifying disease-related biomarkers and new drug targets. Studies have shown that Chinese herbal medicines can achieve therapeutic effects on ALI by affecting

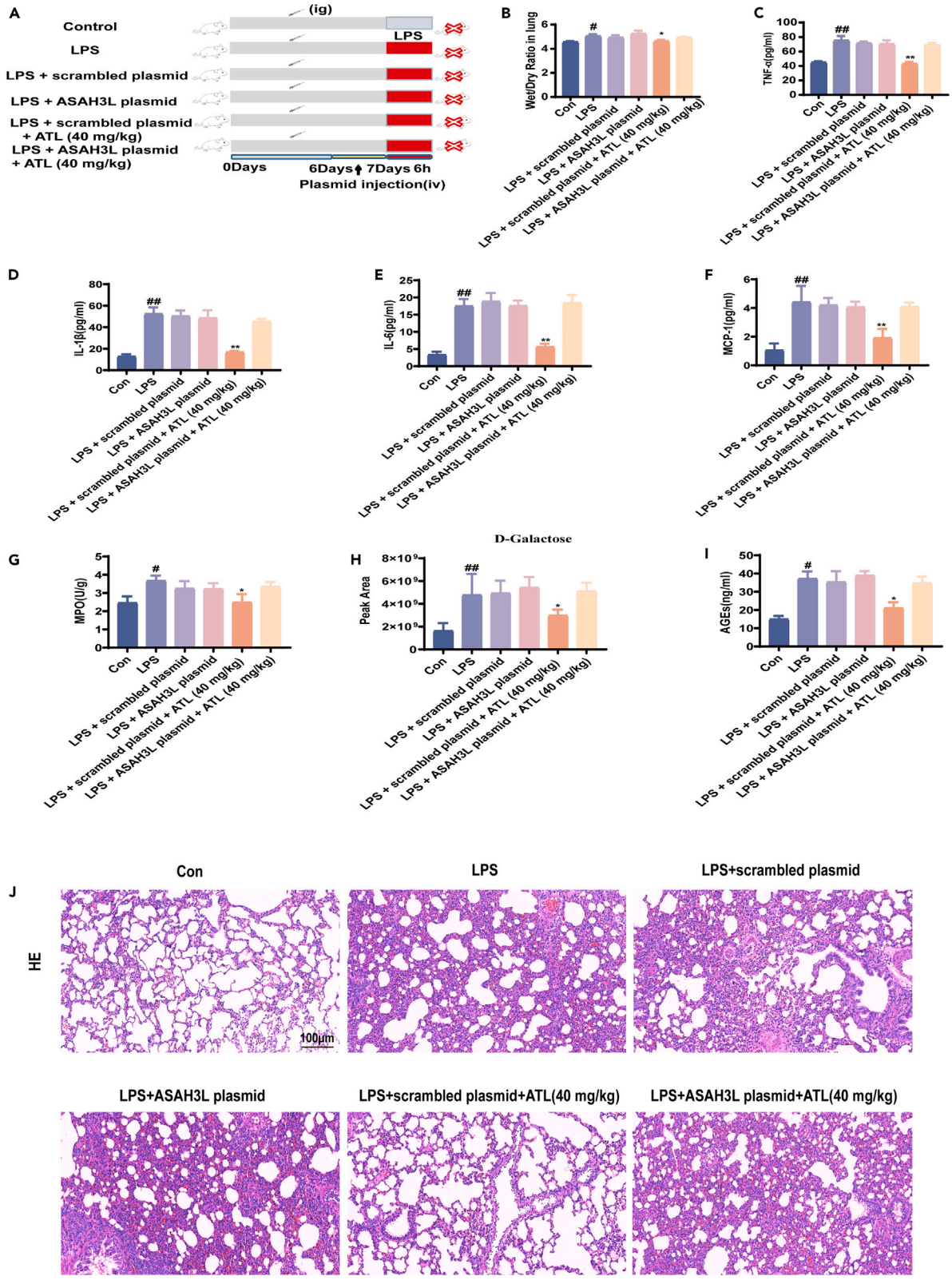
A
Control
LPS
LPS + scrambled plasmid
LPS + ASAH3L plasmid
LPS + scrambled plasmid + ATL (40 mg/kg)
LPS + ASAH3L plasmid + ATL (40 mg/kg)
(ig)
LPS
0Days
6Days
7Days 6h
Plasmid injection(iv)
B
Wet/Dry Ratio in lung
C
TNF-α(pg/ml)
D
IL-1β(pg/ml)
E
IL-6(pg/ml)
F
MCP-1(pg/ml)
G
MPO(U/g)
H
D-Galactose
Peak Area
I
AGEs(ng/ml)
Con
LPS
LPS + scrambled plasmid
LPS + ASAH3L plasmid
LPS + scrambled plasmid + ATL (40 mg/kg)
LPS + ASAH3L plasmid + ATL (40 mg/kg)
J
HE
Con
LPS
LPS+scrambled plasmid
LPS+ASAH3L plasmid
LPS+scrambled plasmid+ATL(40 mg/kg)
LPS+ASAH3L plasmid+ATL(40 mg/kg)
100μm

Figure 9. Effects of ATL on ASAH3L overexpression in rats with ALI

(A) The process flow chart of the overexpression experiments.

(B) Lung W/D ratio. The levels of (C) TNF-α, (D) IL-1β, (E) IL-6, and (F) MCP-1 in BALF as determined by ELISA, $n = 6$. The levels of (G) MPO and (I) AGEs in lung tissues were determined by ELISA, $n = 6$.

(H) The levels of D-galactose in lung tissues were determined by GC-MS, $n = 6$.

(J) Hematoxylin and eosin staining of the lung tissue. The data are expressed as mean ± SEM, $^{\#}p < 0.05$ and $^{\#\#}p < 0.01$ vs. Control; $^{*}p < 0.05$ and $^{**}p < 0.01$ vs. Model.

different metabolites.[36] For example, total flavonoids of Cyclamen significantly affect CYP2J/sEH-mediated arachidonic acid metabolism and reduce inflammatory response and oxidative stress, thus alleviating ALI.[37] As previously described, via transcriptomic analyses, we found that ATL had an effect on various metabolic processes in rats with ALI. Therefore, we further performed metabolomics studies on the rats with ALI. The levels of metabolites such as serine, D-galactose, and D-glucose were significantly upregulated in the model group, and that ATL could modulate the changes in these metabolites. Further enrichment analyses revealed that the metabolic pathways mainly affected by ATL were focused on lactose degradation and galactose metabolism. Studies have shown that under normal conditions, galactose will be converted into glucose and then participate in human metabolism, but when galactose is in excess, it will metabolize ROS and advanced glycation end products (AGEs), thus inducing oxidative stress, inflammatory response and mitochondrial dysfunction.[38,39] Therefore, we speculate that ATL reduces the production of AGEs by inhibiting galactose metabolism, thereby alleviating mitochondrial dysfunction, lowering ROS levels, and further promoting HIF-1α degradation.

ASAH3L stands for Alkaline Ceramidase 2 (ACER2), a type of ceramidase (CDase) that catalyzes the hydrolysis of ceramide to form sphingosine (SPH), which is further phosphorylated to form sphingosine 1-phosphate (S1P). Ceramide (Cer), SPH, and S1P are among the most important biologically active nerve sphingolipid metabolites.[40] ASAH3L regulates cell proliferation, differentiation, survival, and apoptosis and influences the development of related diseases by catalyzing the production of SPH and regulating the balance between Cer and S1P.[41] ASAH3L can induce programmed apoptosis by promoting the hydrolysis of ceramide to SPH, thereby increasing ROS levels.[42,43] Under normal physiological conditions, a portion of ceramide is linked to one or more sugar groups to form glycosphingolipids in the body. This sugar group mainly includes D-galactose, D-glucose, D-acetamidogalactose, and D-acetamidoglucose. When ceramide is hydrolyzed to SPH in excess by ASAH3L, it may lead to the excessive accumulation of D-galactose and D-glucose in the body, which eventually may cause disease.[44,45] In the present study, we found a significant increase in ASAH3L expression in the model group and a significant decrease in ASAH3L expression after the administration of ATL treatment. Furthermore, the results of overexpression experiments indicated that ASAH3L reversed the therapeutic effect of ATL on ALI. Therefore, we speculate that ATL reduces the accumulation of D-galactose *in vivo* by modulating ASAH3L, thereby reducing the production of AGEs and ROS, promoting the degradation of HIF-1α, and attenuating the level of inflammation in rat lungs.

Currently, few studies have been reported about the treatment of ALI with ATL, and its mechanism is not clear. In this study, we first clarified that ATL can improve LPS-induced ALI. Moreover, through the combined analysis of transcriptomics and metabolomics, we have developed for the first time that ASAH3L may be a potential target for the ATL treatment of ALI, providing a new candidate drug and target for the treatment of ALI. However, our study still has many shortcomings, including the fact that we did not use knockouts or inhibitors to further explore the link between ASAH3L and HIF-1α. In addition, how ASAH3L affects the whole process of galactose metabolism remains to be further explored and verified.

In conclusion, our study clarified that ATL can effectively reduce lung inflammation and alleviate ALI. Through transcriptomics and metabolomics analyses, we found that ATL not only inhibits galactose metabolism but also reduces the expression of HIF-1α and ASAH3L. Therefore, in combination with the findings in this study, we suggest that ATL inhibits galactose metabolism by decreasing ASAH3L expression, thereby reducing ROS production, promoting HIF-1α degradation, and reducing the inflammatory response of the lungs to alleviate ALI.

Limitations of the study

In the present study, ASAH3L was revealed to be an important target of atractylodin in the prevention and treatment of acute lung injury for the first time through the use of metabolome, transcriptome, and other multi-omics tools, and overexpression and other molecular biology techniques were used to clearly show that atractylodin mainly modulates ASAH3L to improve the metabolism of galactose and then inhibit the production of ROS, so as to promote the degradation of HIF-1α to alleviate the acute lung injury. However, this article still lacks some verification of previous experiments, such as whether atractylodin can reduce galactose metabolism to inhibit mitochondrial damage and whether atractylodin can promote HIF-1α ubiquitination by reducing ROS production, which needs to be further verified.

RESOURCE AVAILABILITY

Lead contact

Further information and requests for resources and reagents should be directed to and will be fulfilled by the lead contact, Yanju LIU (lyj1965954@hbtcm.edu.cn).

Materials availability

This study did not generate new unique reagents.

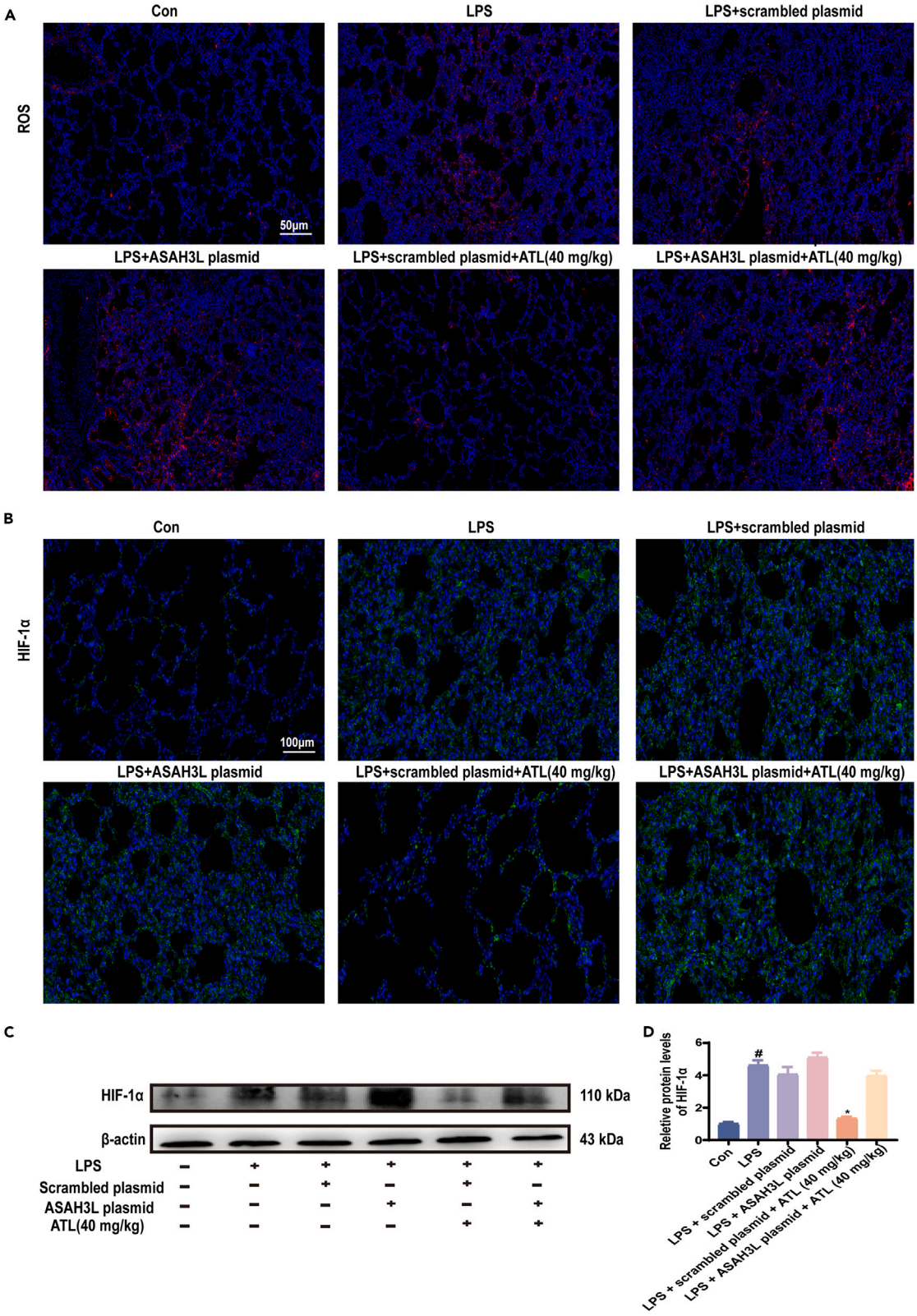
A
Con
LPS
LPS+scrambled plasmid
ROS
50μm
LPS+ASAH3L plasmid
LPS+scrambled plasmid+ATL(40 mg/kg)
LPS+ASAH3L plasmid+ATL(40 mg/kg)
B
Con
LPS
LPS+scrambled plasmid
HIF-1α
100μm
LPS+ASAH3L plasmid
LPS+scrambled plasmid+ATL(40 mg/kg)
LPS+ASAH3L plasmid+ATL(40 mg/kg)
C
HIF-1α
110 kDa
β-actin
43 kDa
LPS
Scrambled plasmid
ASAH3L plasmid
ATL(40 mg/kg)
D
Reletive protein levels of HIF-1α
Con
LPS
LPS + scrambled plasmid
LPS + ASAH3L plasmid
LPS + scrambled plasmid + ATL (40 mg/kg)
LPS + ASAH3L plasmid + ATL (40 mg/kg)

Figure 10. Effects of ASAH3L overexpression on the ROS and HIF-1 signaling pathway

(A) Immunofluorescence staining of ROS in the lung tissue.

(B) Immunofluorescence staining of HIF-1α in the lung tissue.

(C) Western blotting to determine HIF-1α expression in the lung tissue.

(D) Quantitative analysis of HIF-1α levels, $n = 3$. The data are expressed as mean ± SEM, $^{\#}p < 0.05$ vs. Control; $^{*}p < 0.05$ vs. Model.

Data and code availability

- The transcriptomics RNA-seq data have been deposited in the NCBI database and are publicly available as of the date of publication. The metabolomics data have been deposited at Metabolights database and are publicly available as of the date of publication. Accession numbers are listed in the key resources table. All data reported in this article will be shared by the lead contact upon request.
- This article does not report the original code.
- Any additional information required to reanalyze the data reported in this article is available from the lead contact upon request.

ACKNOWLEDGMENTS

This research was funded by the National Natural Science Foundation of China (No. 82074018), the Natural Science Foundation of Hubei Province (2023AFD154), and the Hubei University of Chinese Medicine Project (2023ZXB013).

AUTHOR CONTRIBUTIONS

Kun Shi and Yangxin Xiao conceived and designed the experiments. Kun Shi, Yangxin Xiao, Ying Xie, and Mumujiang Qu performed the experiment. Chang Ke and Yan Wang analyzed the data and prepared figures. Kun Shi wrote the article. Yanju Liu and Linghang Qu provided the financial resources. All authors read and approved the final article.

DECLARATION OF INTERESTS

The authors declare no competing interests.

STAR★METHODS

Detailed methods are provided in the online version of this paper and include the following:

- KEY RESOURCES TABLE
- EXPERIMENTAL MODEL AND STUDY PARTICIPANT DETAILS
  - Animals and treatment
  - Cell culture and treatment
- METHOD DETAILS
  - Lung wet/dry (W/D) ratios and lung injury scores
  - Detection of inflammatory factors
  - Hematoxylin-eosin (HE) staining
  - RNA extraction and RT-qPCR
  - Immunohistochemical (IHC) staining
  - Immunofluorescence staining
  - Western blotting
  - Transcriptome sequencing analysis
  - GC-MS analysis of endogenous metabolites
- QUANTIFICATION AND STATISTICAL ANALYSIS

SUPPLEMENTAL INFORMATION

Supplemental information can be found online at https://doi.org/10.1016/j.isci.2024.110751.

Received: April 7, 2024
Revised: May 30, 2024
Accepted: August 13, 2024
Published: August 31, 2024

REFERENCES

1. Butt, Y., Kurdowska, A., and Allen, T.C. (2016). Acute Lung Injury: A Clinical and Molecular Review. Arch. Pathol. Lab Med. *140*, 345–350. https://doi.org/10.5858/arpa.2015-0519-RA.
2. Wang, S., Lei, P., Feng, Y., Jiang, M., Liu, Z., Shen, T., Ma, S., Wang, L., Guo, X., and Du, S. (2023). Jinyinqingre Oral Liquid alleviates LPS-induced acute lung injury by inhibiting the NF-κB/NLRP3/GSDMD pathway. Chin. J. Nat. Med. *21*, 423–435. https://doi.org/10.1016/s1875-5364(23)60397-8.
3. Long, M.E., Mallampalli, R.K., and Horowitz, J.C. (2022). Pathogenesis of pneumonia and acute lung injury. Clin. Sci. *136*, 747–769. https://doi.org/10.1042/cs20210879.
4. Mokrá, D. (2020). Acute lung injury - from pathophysiology to treatment. Physiol. Res. *69*. S353-s366. https://doi.org/10.33549/physiolres.934602.
5. Fan, E., Brodie, D., and Slutsky, A.S. (2018). Acute Respiratory Distress Syndrome: Advances in Diagnosis and Treatment. JAMA *319*, 698–710. https://doi.org/10.1001/jama.2017.21907.
6. Johnson, E.R., and Matthay, M.A. (2010). Acute lung injury: epidemiology, pathogenesis, and treatment. J. Aerosol Med. Pulm. Drug Deliv. *23*, 243–252. https://doi.org/10.1089/jamp.2009.0775.
7. Evans, C.E. (2022). Hypoxia-Inducible Factor Signaling in Inflammatory Lung Injury and Repair. Cells *11*, 183. https://doi.org/10.3390/cells11020183.

8. McGettrick, A.F., and O'Neill, L.A.J. (2020). The Role of HIF in Immunity and Inflammation. Cell Metab. *32*, 524–536. https://doi.org/10.1016/j.cmet.2020.08.002.
9. Suresh, M.V., Balijepalli, S., Solanki, S., Aktay, S., Choudhary, K., Shah, Y.M., and Raghavendran, K. (2023). Hypoxia-Inducible Factor 1α and Its Role in Lung Injury: Adaptive or Maladaptive. Inflammation *46*, 491–508. https://doi.org/10.1007/s10753-022-01769-z.
10. Vohwinkel, C.U., Hoegl, S., and Eltzschig, H.K. (2015). Hypoxia signaling during acute lung injury. J. Appl. Physiol. *119*, 1157–1163. https://doi.org/10.1152/japplphysiol.00226.2015.
11. Liu, G., and Summer, R. (2019). Cellular Metabolism in Lung Health and Disease. Annu. Rev. Physiol. *81*, 403–428. https://doi.org/10.1146/annurev-physiol-020518-114640.
12. Michaeloudes, C., Bhavsar, P.K., Mumby, S., Xu, B., Hui, C.K.M., Chung, K.F., and Adcock, I.M. (2020). Role of Metabolic Reprogramming in Pulmonary Innate Immunity and Its Impact on Lung Diseases. J. Innate Immun. *12*, 31–46. https://doi.org/10.1159/000504344.
13. Li, L., Cui, H., Zhang, Y., Xie, W., Lin, Y., Guo, Y., Huang, T., Xue, B., Guo, W., Huang, Z., et al. (2023). Baicalin ameliorates multidrug-resistant Pseudomonas aeruginosa induced pulmonary inflammation in rat via arginine biosynthesis. Biomed. Pharmacother. *162*, 114660. https://doi.org/10.1016/j.biopha.2023.114660.
14. Nan, W., Xiong, F., Zheng, H., Li, C., Lou, C., Lei, X., Wu, H., Gao, H., and Li, Y. (2022). Myristoyl lysophosphatidylcholine is a biomarker and potential therapeutic target for community-acquired pneumonia. Redox Biol. *58*, 102556. https://doi.org/10.1016/j.redox.2022.102556.
15. Tang, L., Zhang, S., Zhang, M., Wang, P.J., Liang, G.Y., and Gao, X.L. (2022). Analysis of protective effects of Rosa Roxburghii Tratt fruit polyphenols on lipopolysaccharide-induced acute lung injury through network pharmacology and metabolomics. Food Sci. Nutr. *10*, 4258–4269. https://doi.org/10.1002/fsn3.3019.
16. Jiang, X., Sun, J., Guo, S., Zhao, Z., Chen, Y., Cao, J., Liu, Y., Cheng, G., Tian, L., and Li, Y. (2023). Elsholtzia bodinieri Vaniot ameliorated acute lung injury in mice by regulating pyroptosis, inflammation, oxidative stress and macrophage polarization. J. Ethnopharmacol. *307*, 116232. https://doi.org/10.1016/j.jep.2023.116232.
17. Li, J., Lu, K., Sun, F., Tan, S., Zhang, X., Sheng, W., Hao, W., Liu, M., Lv, W., and Han, W. (2021). Panaxydol attenuates ferroptosis against LPS-induced acute lung injury in mice by Keap1-Nrf2/HO-1 pathway. J. Transl. Med. *19*, 96. https://doi.org/10.1186/s12967-021-02745-1.
18. Qu, L., Lin, X., Liu, C., Ke, C., Zhou, Z., Xu, K., Cao, G., and Liu, Y. (2021). Atractylodin Attenuates Dextran Sulfate Sodium-Induced Colitis by Alleviating Gut Microbiota Dysbiosis and Inhibiting Inflammatory Response Through the MAPK Pathway. Front. Pharmacol. *12*, 665376. https://doi.org/10.3389/fphar.2021.665376.
19. Xu, L., Zhou, Y., Xu, J., Xu, X., Lu, G., Lv, Q., Wei, L., Deng, X., Shen, X., Feng, H., and Wang, J. (2022). Anti-inflammatory, antioxidant and anti-virulence roles of atractylodin in attenuating Listeria monocytogenes infection. Front. Immunol. *13*, 977051. https://doi.org/10.3389/fimmu.2022.977051.
20. Wang, D., Dong, Y., Xie, Y., Xiao, Y., Ke, C., Shi, K., Zhou, Z., Tu, J., Qu, L., and Liu, Y. (2023). Atractylodes lancea Rhizome Polysaccharide Alleviates Immunosuppression and Intestinal Mucosal Injury in Mice Treated with Cyclophosphamide. J. Agric. Food Chem. *71*, 17112–17129. https://doi.org/10.1021/acs.jafc.3c05173.
21. Chang, K.W., Zhang, X., Lin, S.C., Lin, Y.C., Li, C.H., Akhrymuk, I., Lin, S.H., and Lin, C.C. (2021). Atractylodin Suppresses TGF-β-Mediated Epithelial-Mesenchymal Transition in Alveolar Epithelial Cells and Attenuates Bleomycin-Induced Pulmonary Fibrosis in Mice. Int. J. Mol. Sci. *22*, 11152. https://doi.org/10.3390/ijms222011152.
22. Saidi, H., Bérubé, J., Laraba-Djebari, F., and Hammoudi-Triki, D. (2018). Involvement of Alveolar Macrophages and Neutrophils in Acute Lung Injury After Scorpion Envenomation: New Pharmacological Targets. Inflammation *41*, 773–783. https://doi.org/10.1007/s10753-018-0731-9.
23. Shi, K., Xiao, Y., Dong, Y., Wang, D., Xie, Y., Tu, J., Xu, K., Zhou, Z., Cao, G., and Liu, Y. (2022). Protective Effects of Atractylodis lancea Rhizoma on Lipopolysaccharide-Induced Acute Lung Injury via TLR4/NF-κB and Keap1/Nrf2 Signaling Pathways In Vitro and In Vivo. Int. J. Mol. Sci. *23*, 16134. https://doi.org/10.3390/ijms232416134.
24. Batah, S.S., and Fabro, A.T. (2021). Pulmonary pathology of ARDS in COVID-19: A pathological review for clinicians. Respir. Med. *176*, 106239. https://doi.org/10.1016/j.rmed.2020.106239.
25. Alghetaa, H., Mohammed, A., Sultan, M., Busbee, P., Murphy, A., Chatterjee, S., Nagarkatti, M., and Nagarkatti, P. (2018). Resveratrol protects mice against SEB-induced acute lung injury and mortality by miR-193a modulation that targets TGF-β signalling. J. Cell Mol. Med. *22*, 2644–2655. https://doi.org/10.1111/jcmm.13542.
26. Fanelli, V., and Ranieri, V.M. (2015). Mechanisms and clinical consequences of acute lung injury. Ann. Am. Thorac. Soc. *12*, S3–S8. https://doi.org/10.1513/AnnalsATS.201407-340MG.
27. Hsieh, P.C., Wu, Y.K., Yang, M.C., Su, W.L., Kuo, C.Y., and Lan, C.C. (2022). Deciphering the role of damage-associated molecular patterns and inflammatory responses in acute lung injury. Life Sci. *305*, 120782. https://doi.org/10.1016/j.lfs.2022.120782.
28. Aegerter, H., Lambrecht, B.N., and Jakubzick, C.V. (2022). Biology of lung macrophages in health and disease. Immunity *55*, 1564–1580. https://doi.org/10.1016/j.immuni.2022.08.010.
29. Park, I., Kim, M., Choe, K., Song, E., Seo, H., Hwang, Y., Ahn, J., Lee, S.H., Lee, J.H., Jo, Y.H., et al. (2019). Neutrophils disturb pulmonary microcirculation in sepsis-induced acute lung injury. Eur. Respir. J. *53*, 1800786. https://doi.org/10.1183/13993003.00786-2018.
30. Wang, K., Wang, M., Liao, X., Gao, S., Hua, J., Wu, X., Guo, Q., Xu, W., Sun, J., He, Y., et al. (2022). Locally organised and activated Fth1(hi) neutrophils aggravate inflammation of acute lung injury in an IL-10-dependent manner. Nat. Commun. *13*, 7703. https://doi.org/10.1038/s41467-022-35492-y.
31. Lee, J.W., Seo, K.H., Ryu, H.W., Yuk, H.J., Park, H.A., Lim, Y., Ahn, K.S., and Oh, S.R. (2018). Anti-inflammatory effect of stem bark of Paulownia tomentosa Steud. in lipopolysaccharide (LPS)-stimulated RAW264.7 macrophages and LPS-induced murine model of acute lung injury. J. Ethnopharmacol. *210*, 23–30. https://doi.org/10.1016/j.jep.2017.08.028.
32. Malkov, M.I., Lee, C.T., and Taylor, C.T. (2021). Regulation of the Hypoxia-Inducible Factor (HIF) by Pro-Inflammatory Cytokines. Cells *10*, 2340. https://doi.org/10.3390/cells10092340.
33. Watts, E.R., and Walmsley, S.R. (2019). Inflammation and Hypoxia: HIF and PHD Isoform Selectivity. Trends Mol. Med. *25*, 33–46. https://doi.org/10.1016/j.molmed.2018.10.006.
34. Chin, B.Y., Jiang, G., Wegiel, B., Wang, H.J., Macdonald, T., Zhang, X.C., Gallo, D., Cszimadia, E., Bach, F.H., Lee, P.J., and Otterbein, L.E. (2007). Hypoxia-inducible factor 1alpha stabilization by carbon monoxide results in cytoprotective preconditioning. Proc. Natl. Acad. Sci. USA *104*, 5109–5114. https://doi.org/10.1073/pnas.0609611104.
35. Zhao, S., Gao, J., Li, J., Wang, S., Yuan, C., and Liu, Q. (2021). PD-L1 Regulates Inflammation in LPS-Induced Lung Epithelial Cells and Vascular Endothelial Cells by Interacting with the HIF-1α Signaling Pathway. Inflammation *44*, 1969–1981. https://doi.org/10.1007/s10753-021-01474-3.
36. He, Y.Q., Zhou, C.C., Yu, L.Y., Wang, L., Deng, J.L., Tao, Y.L., Zhang, F., and Chen, W.S. (2021). Natural product derived phytochemicals in managing acute lung injury by multiple mechanisms. Pharmacol. Res. *163*, 105224. https://doi.org/10.1016/j.phrs.2020.105224.
37. Zhang, J., Zhang, M., Zhang, W.H., Zhu, Q.M., Huo, X.K., Sun, C.P., Ma, X.C., and Xiao, H.T. (2022). Total flavonoids of Inula japonica alleviated the inflammatory response and oxidative stress in LPS-induced acute lung injury via inhibiting the sEH activity: Insights from lipid metabolomics. Phytomedicine *107*, 154380. https://doi.org/10.1016/j.phymed.2022.154380.
38. Kumar, H., Bhardwaj, K., Valko, M., Alomar, S.Y., Alwasel, S.H., Cruz-Martins, N., Dhanjal, D.S., Singh, R., Kuča, K., Verma, R., and Kumar, D. (2022). Antioxidative potential of Lactobacillus sp. in ameliorating D-galactose-induced aging. Appl. Microbiol. Biotechnol. *106*, 4831–4843. https://doi.org/10.1007/s00253-022-12041-7.
39. Qi, X., and Tester, R.F. (2019). Fructose, galactose and glucose - In health and disease. Clin. Nutr. ESPEN *33*, 18–28. https://doi.org/10.1016/j.clnesp.2019.07.004.
40. Parveen, F., Bender, D., Law, S.H., Mishra, V.K., Chen, C.C., and Ke, L.Y. (2019). Role of Ceramidases in Sphingolipid Metabolism and Human Diseases. Cells *8*, 1573. https://doi.org/10.3390/cells8121573.
41. Coant, N., Sakamoto, W., Mao, C., and Hannun, Y.A. (2017). Ceramidases, roles in sphingolipid metabolism and in health and disease. Adv. Biol. Regul. *63*, 122–131. https://doi.org/10.1016/j.jbior.2016.10.002.
42. Dielschneider, R.F., Henson, E.S., and Gibson, S.B. (2017). Lysosomes as Oxidative Targets for Cancer Therapy. Oxid. Med. Cell. Longev. *2017*, 3749157. https://doi.org/10.1155/2017/3749157.
43. Ueda, N. (2017). Sphingolipids in Genetic and Acquired Forms of Chronic Kidney Diseases.

Curr. Med. Chem. *24*, 1238–1275. https://doi.org/10.2174/0929867324666170112114525.

44. Balram, A., Thapa, S., and Chatterjee, S. (2022). Glycosphingolipids in Diabetes, Oxidative Stress, and Cardiovascular Disease: Prevention in Experimental Animal Models. Int. J. Mol. Sci. *23*, 15442. https://doi.org/10.3390/ijms232315442.
45. Furukawa, K., Ohmi, Y., Kondo, Y., Ohkawa, Y., Tajima, O., and Furukawa, K. (2015). Regulatory function of glycosphingolipids in the inflammation and degeneration. Arch. Biochem. Biophys. *571*, 58–65. https://doi.org/10.1016/j.abb.2015.02.007.
46. Shi, K., Wang, Y., Xiao, Y., Tu, J., Zhou, Z., Cao, G., and Liu, Y. (2023). Therapeutic effects and mechanism of Atractylodis rhizoma in acute lung injury: Investigation based on an Integrated approach. Front. Pharmacol. *14*, 1181951. https://doi.org/10.3389/fphar.2023.1181951.
47. Qu, L., Shi, K., Xu, J., Liu, C., Ke, C., Zhan, X., Xu, K., and Liu, Y. (2022). Atractylenolide-1 targets SPHK1 and B4GALT2 to regulate intestinal metabolism and flora composition to improve inflammation in mice with colitis. Phytomedicine *98*, 153945. https://doi.org/10.1016/j.phymed.2022.153945.
48. Li, Q., Fu, X., Yuan, J., and Han, S. (2021). Contribution of Thrombospondin-1 and -2 to Lipopolysaccharide-Induced Acute Respiratory Distress Syndrome. Mediators Inflamm. *2021*, 8876484. https://doi.org/10.1155/2021/8876484.
49. Ji, T., Chen, M., Liu, Y., Jiang, H., Li, N., and He, X. (2023). Artesunate alleviates intestinal ischemia/reperfusion induced acute lung injury via up-regulating AKT and HO-1 signal pathway in mice. Int. Immunopharmacol. *122*, 110571. https://doi.org/10.1016/j.intimp.2023.110571.
50. Wang, Y., Shi, K., Tu, J., Ke, C., Chen, N., Wang, B., Liu, Y., and Zhou, Z. (2023). Atractylenolide III Ameliorates Bile Duct Ligation-Induced Liver Fibrosis by Inhibiting the PI3K/AKT Pathway and Regulating Glutamine Metabolism. Molecules *28*, 5504. https://doi.org/10.3390/molecules28145504.
51. Shi, K., Qu, L., Lin, X., Xie, Y., Tu, J., Liu, X., Zhou, Z., Cao, G., Li, S., and Liu, Y. (2019). Deep-Fried Atractylodis Rhizoma Protects against Spleen Deficiency-Induced Diarrhea through Regulating Intestinal Inflammatory Response and Gut Microbiota. Int. J. Mol. Sci. *21*, 124. https://doi.org/10.3390/ijms21010124.
52. Qu, L., Liu, C., Ke, C., Zhan, X., Li, L., Xu, H., Xu, K., and Liu, Y. (2022). Atractylodes lancea Rhizoma Attenuates DSS-Induced Colitis by Regulating Intestinal Flora and Metabolites. Am. J. Chin. Med. *50*, 525–552. https://doi.org/10.1142/s0192415x22500203.

STAR★METHODS

KEY RESOURCES TABLE

REAGENT or RESOURCE	SOURCE	IDENTIFIER
Antibodies		
β-actin	Solarbio	Cat# K200058M
MPO	Abcam	Cat# ERP20257
HIF-1α	Abcam	Cat# ab179483
MCP-1	Abcam	Cat# ab7202
ASAH3L	Thermo Fisher	Cat# PA575832
Ly-6G	Abcam	Cat# ab238132
F4/80	Abcam	Cat# ab300421
HRP secondary antibody	Abcam	Cat# ab205718
Biological samples		
THP-1 cells	Procell Life Science	N/A
Male SD rats	Animal Experiment Center of Hubei Province	SCXK (E) 2023-0013
Chemicals, peptides, and recombinant proteins		
DAPI	Sigma	Cat# S7113
PI	Beyotime	Cat# ST511
Hoechst 33258	Beyotime	Cat# C1018
FBS	Gibco	Cat# 10099-141
RPMI-1640	Gibco	Cat# 11875119
LPS	Solarbio	Cat# L8880
PMA	MedChemExpress	Cat# HY-18739
DMSO	Merck	Cat# D2650
Cocktail	Sigma	Cat #539132
ECL	Beyotime	Cat# P0018S
RIPA	Servicebio	Cat# G2002
TRIZOL	BIOLOGY	Cat# BOLG601
Pyridine	Sigma	Cat# SHBK6453
Dexamethasone	Sigma	Cat# D4902
methoxyamine hydrochloride	Sigma	Cat# BCBZ8981
Atractylodin	Chengdu Push	Cat# PU0490-0025
Transfection reagents	Engreen	Cat# 18668-11-1
Critical commercial assays		
Cell counting kit-8	AbMole	Cat# M4839
Rat-TNF-a ELISA kits	ABclonal	Cat# RK00029
Rat-IL-1β ELISA kits	ABclonal	Cat# RK00009
Rat-IL-6 ELISA kits	ABclonal	Cat# RK00020
Rat-MCP-1 ELISA kits	Elabscience	Cat# E-EL-R0633c
Rat-MPO ELISA kits	Elabscience	Cat# E-BC-K074-M
Human-TNF-a ELISA kits	Elabscience	Cat# E-EL-H0109c
Human-IL-1β ELISA kits	Elabscience	Cat# E-EL-H0149c
Human-IL-6 ELISA kits	Elabscience	Cat# E-EL-H6156
Human—MCP-1 ELISA kits	Elabscience	Cat# E-EL-H6005

(*Continued on next page*)

Continued

REAGENT or RESOURCE	SOURCE	IDENTIFIER
Quant-iT PicoGreen dsDNA Assay Kit	Thermo Fisher	Cat# P7589
MiSeq Reagent Kit V3	Illumina	Cat# MS-102-3003
Deposited data		
Transcriptomics data	NCBI database	PRJNA1101692
Metabolomic data	Metabolights database	MTBLS9948

EXPERIMENTAL MODEL AND STUDY PARTICIPANT DETAILS

Animals and treatment

Male SD rats (5–6 weeks, 160 ± 20 g) were obtained from the Animal Experiment Center of Hubei Province. The animal license is SCXK (E) 2023-0013. All rats were kept in animal rooms with suitable temperatures, with adequate sterile water and food, light for 12 h and darkness for 12 h per day. All experimental procedures were in accordance with ethical requirements and approved by the Ethics Committee of Hubei University of Traditional Chinese Medicine (Approval No. NO.00272049, November 9, 2022). A total of 60 rats were randomly distributed into 5 groups: control, model, ATL (10 mg/kg), ATL (40 mg/kg), and Dex (5 mg/kg), with 12 rats in each group. After acclimatization feeding for 3 days, each dosing group was administered the corresponding drug by gavage for 7 days, while the control group and model group received the same dose of solvent. After 7 days of gavage, all groups except the control group were subjected to a tracheal drip of LPS (5 mg/kg) to induce ALI.[46] After 6 h, the rats were euthanized with sodium pentobarbital. Lung tissues and bronchoalveolar lavage fluid (BALF) were then collected and stored for further use. The ATL standard was dissolved by sonication with 5% DMSO, 30% PEG300, 10% Tween 80, and 55% double-distilled water.

In order to further investigate the role of ASAH3L overexpression in ALI rats treated with ATL, 72 rats were distributed into 6 groups: control group, LPS group, LPS + scrambled plasmid group, LPS + ASAH3L plasmid group, LPS + scrambled plasmid + ATL (40 mg/kg) group, and LPS + ASAH3L plasmid + ATL (40 mg/kg) group, with 12 rats in each group. The plasmid was mixed 1:2 with Entranster *in vivo* transfection reagent following the manufacturer's instructions and injected into rats via the tail vein 24 h before LPS administration to induce ALI.[47,48] The other procedures were consistent with the previous animal experiments.

Cell culture and treatment

THP-1 cells were acquired from Procell Life Science & Technology Co., Ltd (Wuhan, China). The cells were cultured under the RPMI 1640 medium with 10% fetal bovine serum (FBS, Gibco, Grand Island, NY, USA). THP-1 cells were seeded in 96-well plates, after which the cells were co-incubated with PMA (100 ng/mL) and ATL (0, 5, 10, 20, 40, 80, and 160 μM) for 24 h. The toxic effects of different concentrations of ATL on THP-1 cells were determined using a CCK-8 kit.

METHOD DETAILS

Lung wet/dry (W/D) ratios and lung injury scores

The first six rats in each group were not subjected to alveolar lavage; the left lung tissue was removed, rinsed with PBS to remove residual blood, and then blotted dried on filter paper, weighed, and recorded as wet weight. The tissue was then placed in an oven at 80°C for 48 h, weighed again, and recorded as dry weight.[23] W/D ratio of lungs = wet weight/dry weight.

The lung injury was assessed according to the following items: inflammatory cell infiltration to the airspace or alveolar space, hyaline membrane formation, alveolar septal thickening, and pulmonary hemorrhage. The tissues were scored as follows: no injury, 0; mild to moderate injury, 0.1–2.5; and severe injury, 2.6–4.0.[49]

Detection of inflammatory factors

In the *in vivo* experiments, after alveolar lavage of the left lungs of the six remaining rats in each group, we obtained the BALF or lung tissues, which were then assayed according to the kit instructions. The kits for TNF-α (E-EL-R2856c), IL-1β (E-EL-R0012c), IL-6 (E-EL-R0015c), MCP-1 (E-EL-R0633c), and MPO (E-BC-K074-M) in rat species were purchased from the Elabscience Biotechnology Co, Ltd. (Wuhan, China). The kit for advanced glycation end products (AGEs) (RK06498) was obtained from ABclonal Technology Co., Ltd. (Wuhan, China). In the *in vitro* experiments, THP-1 cells (5×10^5 cells/well) were seeded in well plates and co-incubated with PMA (100 ng/mL) for 24 h. After removing the supernatant, LPS (1 μg/mL) and ATL (10, 20, and 40 μM) or Dex (10 μM) were added for 24 h of incubation. We gathered cell supernatants and then followed the kit instructions for the assay. The kits for TNF-α (E-EL-H0109c), IL-1β (E-EL-H0149c), IL-6 (E-EL-H6156), and MCP-1 (E-EL-H6005) in human species were purchased from the Elabscience Biotechnology Co, Ltd. (Wuhan, China).

Hematoxylin-eosin (HE) staining

We fixed the middle lobe tissue of the right lung with 4% paraformaldehyde for 24 h; the tissues were then embedded in paraffin wax, sectioned, stained with H&E and finally observed under a light microscope.[23]

RNA extraction and RT-qPCR

Total RNA in samples were extracted using FastPure Cell/Tissue Total RNA Isolation Kit V2 (Vazyme Biotech Co., Ltd, Nanjing, China).[50] The RNA was reverse-transcribed into cDNA. Primers were obtained from the Tsingke Biotechnology Co., Ltd. All gene expression values were normalized to β-actin expression and calculated using the $2^{-\Delta\Delta CT}$ method.[23] The specific primer sequences for all genes quantified are listed in Table S1.

Immunohistochemical (IHC) staining

We fixed the lung tissues in 4% paraformaldehyde overnight, paraffin-embedded and sectioned the tissues, and incubated them overnight with MPO and MCP-1 primary antibodies (1:1000).[46] Then, incubate the tissue with secondary antibody (1:5000) at room temperature. Positive cells were stained brown with 3,3 ′- diaminobenzidine (DAB).

Immunofluorescence staining

We fixed the lung tissues in 4% paraformaldehyde overnight, paraffin-embedded and sectioned the tissues, and incubated them overnight with F4/80 (ab300421; Abcam Inc., Cambridge, MA, USA) and Ly-6G (ab238132; Abcam Inc., Cambridge, MA, USA) primary antibodies (1:1000).[51] After washing three times with PBS, the tissue was incubated with secondary antibody (1:5000) for 2 h at room temperature. Cell nuclei were stained using DAPI and the tissues were then observed via fluorescence microscopy.

Western blotting

Lung tissues were cryomilled using a cryomill, and subsequently protein concentrations were determined with a bicinchoninic acid (BCA) kit (Elabscience Biotechnology Co., Ltd., Wuhan, China).[52] Proteins were separated by sodium dodecyl sulfate-polyacrylamide gel electrophoresis and transferred onto a PVDF membrane. The membranes were blocked with 5% skim milk powder dissolved in Tris-buffered saline containing 0.1% Tween 20 (TBST) for 2 h at room temperature. The membranes were then washed three times with TBST, for 5 min each time, and incubated with the primary antibody (1:1000) at 4°C overnight. The following day, the membranes were washed three times with TBST, for 5 min each time, and incubated with the secondary antibody (1:5000) for 2 h at room temperature.[46] The results were analyzed using the enhanced chemiluminescence detection kit (Vazyme Biotech Co., Ltd., Nanjing, China).

Transcriptome sequencing analysis

Total RNA was extracted and purified from rat lung tissues of control, model, and ATL 40 mg/kg groups using Qiagen RNA extraction and purification kit.[47] The library construction kit used was Illumina's NEBNext UltraTM RNA Library Preparation Kit. All data analysis is performed on the following website: https://biosys.bgi.com/.

GC-MS analysis of endogenous metabolites

30 mg of lung tissue was weighed in an enzyme-free tube and 1 mL of methanol was added. The tissue sample was ground under a cryogenic pulverizer, then centrifuged to collect the supernatant and blow-dried under nitrogen. Then perform derivatization processing, and finally 150 μL sample was added to a lined test tube for testing.[46] All metabolomic data analysis was performed using Metaboanalyst 5.0 (https://www.metaboanalyst.ca/).

QUANTIFICATION AND STATISTICAL ANALYSIS

Data processing and analysis were accomplished with GraphPad 8.0 and SPSS 22.0. Shapiro-Wilk test was used to evaluate the normal distribution and the chi-square test. One-way analysis of variance (ANOVA) was performed on normally distributed data, and the results are shown as mean ± standard error of the mean (SEM). The analysis of samples with nonnormal distribution or uneven variance was performed using Kruskal-Wallis, and the results are shown as median (quartiles).[18] $p < 0.05$ indicated significant differences.